

MASTER

Mechanical design and construction of a 5 DOF haptic master device for an eye-surgery robot

Grasman, J.H.

Award date:
2008

[Link to publication](#)

Disclaimer

This document contains a student thesis (bachelor's or master's), as authored by a student at Eindhoven University of Technology. Student theses are made available in the TU/e repository upon obtaining the required degree. The grade received is not published on the document as presented in the repository. The required complexity or quality of research of student theses may vary by program, and the required minimum study period may vary in duration.

General rights

Copyright and moral rights for the publications made accessible in the public portal are retained by the authors and/or other copyright owners and it is a condition of accessing publications that users recognise and abide by the legal requirements associated with these rights.

- Users may download and print one copy of any publication from the public portal for the purpose of private study or research.
- You may not further distribute the material or use it for any profit-making activity or commercial gain

Mechanical design and construction
of a 5 DOF haptic master device
for an eye-surgery robot

J.H. Grasman

DCT 2008.111

Master's Thesis

Supervisor: Prof. dr. ir. M. Steinbuch

Coaches: Dr. ir. P.C.J.N. Rosielle

Ir. R. Hendrix

EINDHOVEN UNIVERSITY OF TECHNOLOGY
DEPARTMENT OF MECHANICAL ENGINEERING
SECTION CONTROL SYSTEMS TECHNOLOGY

Eindhoven, August 2008

Summary

Nowadays all eye-surgeries are performed by hand. Before a surgeon is authorised to perform these very complex operations, years of study and practice are necessary. The surgeon must have very accurate hand movements. During aging of the surgeon, hand tremor increases and most surgeons will not be able to perform the surgery around their mid-fifties. Besides this, the unergonomic operating position often results in early disability of the surgeon. These problems have led to the idea of designing a master-slave robot for eye surgery. A project is started called Eye Rhas, which stands for Eye Robot for haptic assisted surgery (haptic means pertaining to the sense of touch).

The surgeon will have two haptic interfaces in his hands, which are approximately 10 times larger than the instruments in the eye of the patient. With this master (pens) he controls the slave that manipulates instruments within the eye of the patient. It has the same 5 degrees of freedom (DOF) as the instrument: φ , ψ , θ , z and button stroke. The surgeon now moves his hand virtually within the eye of the patient. A visualisation system gives the surgeon information about the slave movements. By measuring the forces on the instrument, force feedback can be given to the surgeon with the haptic pen, giving the surgeon a better feeling of his operation actions.

In this thesis this haptic interface is designed and a prototype has been built.

The haptic characteristic of the pen is created by an actuator per DOF, which can generate force feedback to the hand of the surgeon. The size of the realised forces is based on presumptions made before this project started. To obtain the best haptic feeling, there should be no noticeable disturbance forces. An average human being is able to notice a force deviation of 7% of the total applied force. Friction analysis of the design indicates that the friction will be below this percentage and therefore will not be felt by the surgeon.

The highest precision of the hand movement of a surgeon is approximately $5 \cdot 10^{-5} m$. The haptic pen is able to measure this movement and better; the resolution of the pen in each DOF is at least $3 \cdot 10^{-5} m$. The finite stiffness of the pen causes a deviation between actual hand movement and measurement under static and dynamic loading. A first stiffness analysis of all separate parts indicates that the total stiffness is sufficient for the stated precision.

Testing of the prototype to confirm the friction and stiffness analysis has not been done yet.

Contents

Summary	iii
Contents	v
1 Introduction	1
2 Eye Rhas	3
2.1 Vitreo-retinal surgery	3
2.2 Layout master-slave robot	5
3 Requirements of the haptic pen	7
3.1 Degrees of freedom	7
3.2 Ranges	8
3.3 Force feedback	8
3.4 Resolution	9
3.5 Stiffness	9
4 Haptic pen design	11
4.1 Pen composition	11
4.2 φ and ψ part	14
4.2.1 Direct drive	14
4.2.2 Motor choice	15
4.2.3 Bearing stiffness and load	16
4.2.4 Resolution	18
4.2.5 Cable	19
4.2.6 Range	19
4.3 θ -z part	20
4.3.1 Parallel θ -z drive	21
4.3.2 Motor choice	21

4.3.3 Z-drive	22
4.3.3.1 Z-transmission	22
4.3.3.2 Anti backlash gear.....	23
4.3.3.3 Tooth strength.....	24
4.3.3.4 θ -uncoupling.....	24
4.3.3.5 Rotation/translation bearing stiffness and load.....	24
4.3.3.6 Rack guiding.....	25
4.3.3.7 Z-Resolution	26
4.3.3.8 Z-Range.....	26
4.3.4 θ -movement	27
4.3.4.1 θ -Transmission.....	27
4.3.4.2 Anti backlash gear.....	27
4.3.4.3 Tooth strength.....	28
4.3.4.4 Z-uncoupling.....	28
4.3.4.5 θ -Resolution.....	29
4.3.4.6 θ -Range	29
4.3.5 Friction in θ and z	29
4.4 Button Part.....	31
4.4.1 Drive.....	32
4.4.2 Backlash	33
4.4.3 Resolution.....	33
4.4.3 Cable	33
4.4.4 Button fastening	34
4.5 Weight compensation	35
4.5.1 φ and ψ compensation	35
4.5.2 θ -compensation	38
4.5.3 Z-compensation.....	38
4.6 Performance.....	40
5 Conclusions and recommendations	43
Bibliography	45
A Datasheets purchased parts	47
A1 φ and ψ brushless Kollmorgen motor.....	47
A2 φ and ψ Scancon encoder.....	49
A3 θ and z brushless Maxon motor	51
A4 θ and z Scancon encoder.....	52
A4 button brushless Maxon motor.....	54
B Friction calculations	55
B1 φ -part	55
B2 ψ -part	56
B3 Z-friction.....	56
B4 θ -friction	57
B5 Button part	57

C Stiffness calculations	59
D Cable wrapping	73
D1 φ and ψ cable wrapping	73
D2 θ -z cable wrapping	75
E Tooth strength calculations	77
E1 Z-drive	78
E2 θ -drive	79
F Angular button acceleration	80
List of symbols	81
Acknowledgement	85

1 Introduction

Sight is generally considered to be the most important sense we have. Prevention from losing it is an important, but very difficult task. Interestingly, instruments of eye surgery dating back to the ancient Roman times have been discovered by archaeologists. Fortunately, there have been incredible improvements in eye surgery since that time. Smaller instruments, better medicines and new techniques lead to better results, however all surgeries are still performed by hand.

Because of the complexity of eye surgery, years of study and practice are necessary before a surgeon is authorized to perform eye surgery. Around his mid-fifties, the surgeon will not be able to do this surgery anymore. Due to the increase of tremor in his hands, he is not capable of performing the very accurate tasks anymore. Besides this, the unergonomic operating position often results in early disability of the surgeon.

The first generation of surgical master-slave robots are already being installed in an number of operating rooms around the world. However, eye surgery robots do not exist yet.

The lack of haptic feedback (haptic means pertaining to the sense of touch) in the robots limit their performance and a lot of research in this field is deployed nowadays [1], [2].

The problems in eye surgery have led to the idea of designing a master-slave robot for eye surgery. The surgeon will have two haptic interfaces in his hands. With this master he controls a slave that manipulates instruments within the eye of the patient. A visualisation system gives the surgeon information about the slave movements. By measuring the forces between the instrument and the slave, force feedback can be given to the surgeon with the haptic interfaces.

Tremor can be eliminated, scaling of movements and haptic feedback can result in higher precision and an ergonomic position can be realised.

A cooperative project¹ between TNO², AMC³ and TU/e⁴ is started, called Eye Rhas (Eye-Robot-for-haptic-assisted-surgery). Ir. H.C.M. Meenink is designing the slave, while ir. R. Hendix is designing the master, both for their doctorate research.

This thesis describes a part of the master: the mechanical design and construction of the haptic interface for an eye surgery robot.

¹ Supported by IOP Precision Technology, an innovation driven program of SenterNovem and the Ministry of Economic Affairs

² Toegepast Natuurwetenschappelijk Onderzoek (Applied Scientific Research)

³ Amsterdam Medisch Centrum (Amsterdam Medical Centre)

⁴ Technische Universiteit Eindhoven (Eindhoven University of Technology)

2 Eye Rhas

The Eye-robot-for-haptic-assisted-surgery is expected to have multiple advantages over the present surgery by hand. The robot will be specialized in vitreo-retinal surgery. This type of surgery will be explained and then the layout of the master-slave robot is shown and the advantages are discussed.

2.1 Vitreo-retinal surgery

Epiretinal membrane peeling is a procedure which includes most of the actions used at vitreo-retinal surgery. This procedure will be used to explain this type of eye surgery. In figure 2.1 the inside and outside of the eye is shown, where important parts are indicated.

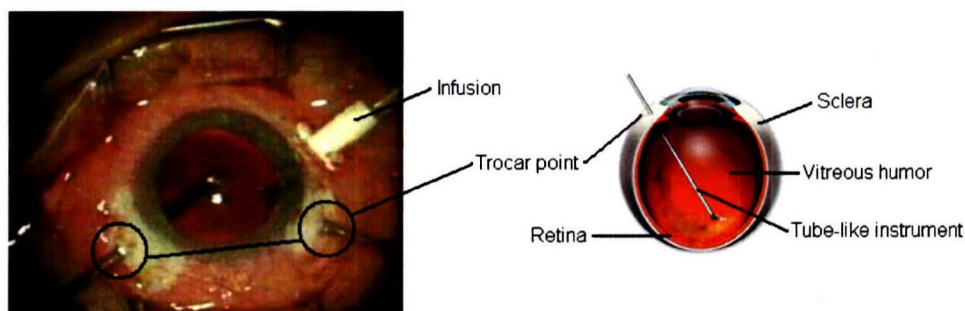


Figure 2.1: outside and inside of the eye

The epiretinal membrane is located just over the retina and has a thickness of approximately 5 μm . Occasionally, traction of this membrane causes deformation of the retina that is attached to it, resulting in loss of vision. Goal of the procedure is peeling the epiretinal membrane and removing this from the eye.

To gain access to the eye, small incisions at the sclera are made, called trocar points. Usually a small tube, the trocar, is placed in each hole during surgery, which makes entering the eye again with an instrument easier.

Before peeling can take place, first the vitreous humor has to be removed with a vitrector. The viscosity of the vitreous humor can be compared with the white of an egg and is lightly attached to the epiretinal membrane. The vitrector uses suction in combination with cutting and thereby deporting the humor in small portions.

Near the retina high precision movements are required. Touching the retina will consequently result in vision loss and abrupt vitrector movements along the retina may cause retinal detachment.

In figure 2.2 an ophthalmologist is shown during eye surgery. He constantly uses a microscope over the eye that can switch between looking at the outside of the eye and looking through the patients lens to obtain an image of the inside of the eye. He uses a light pipe for a better image.

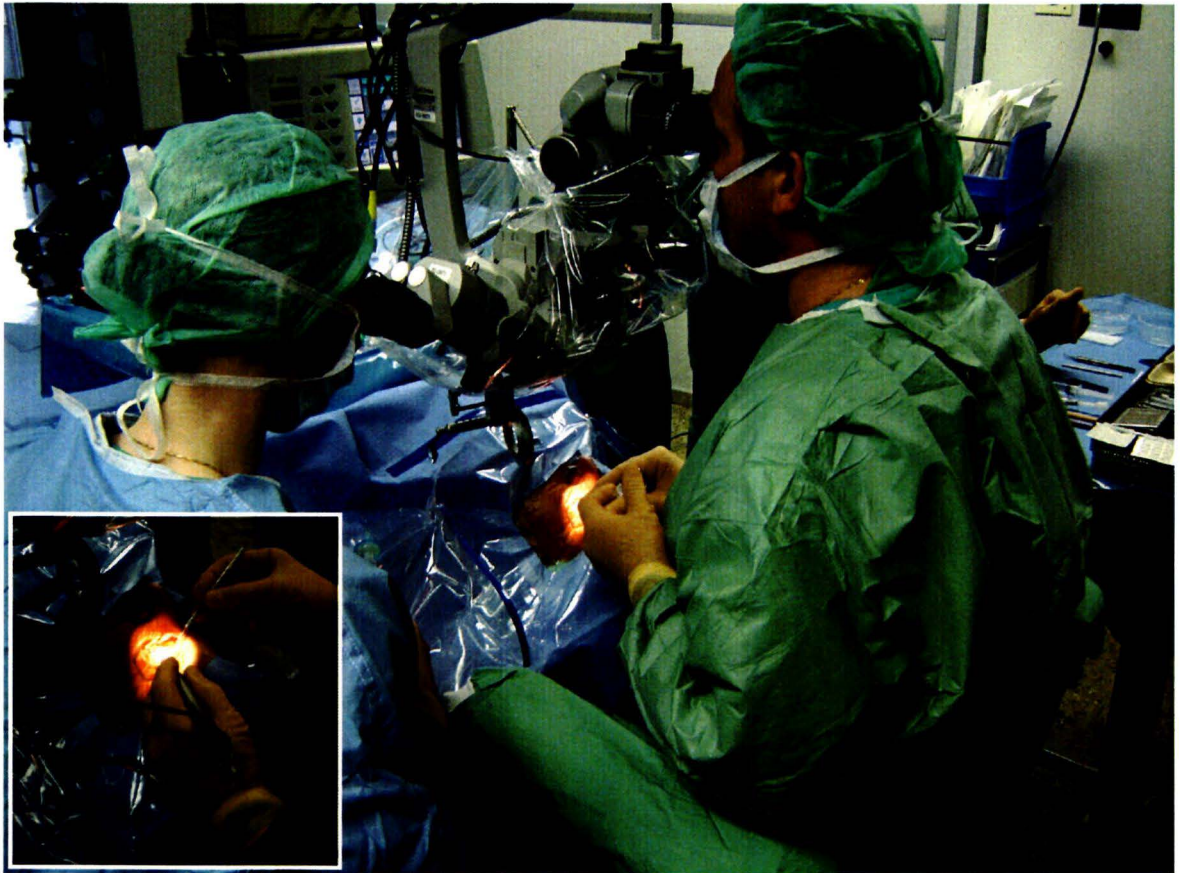


Figure 2.2: An ophthalmologist during eye surgery

An infusion is placed in the eye to control the inside pressure during the whole surgery. After vitrectomy the epiretinal peeling starts. Edges of the membrane are exposed by inserting a coloured liquid. Using a gripper and cutter, the membrane is peeled and removed from the eye. The fixed position of the patients head and the microscope above it lead to an unergonomic posture of the surgeon: almost no back support and body movement during the whole operation (approximately one hour). The surgeon must have very accurate hand movements. Around his mid-fifties the increased tremor of his hands often leads to early retirement.

2.2 Layout master-slave robot

In figure 2.3 a layout of the entire master-slave robot is shown.

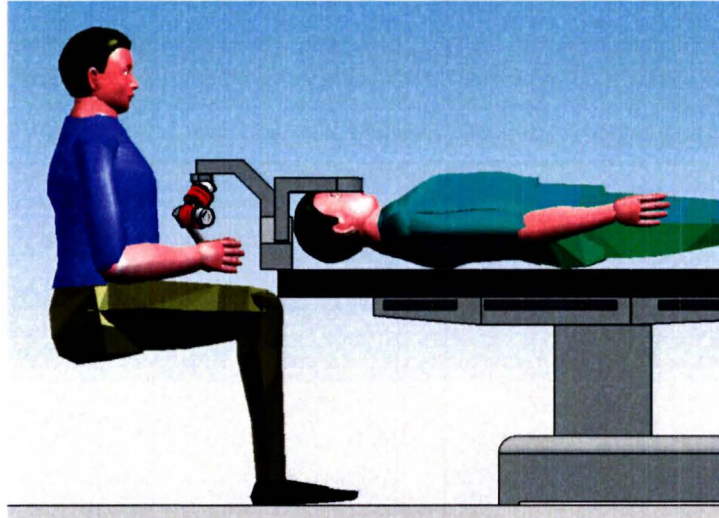


Figure 2.3: Layout master-slave robot

At the left side the surgeon holds a haptic pen in each hand. By moving the haptic pens, the surgeon controls the slave that is positioned around the patients head. The slave manipulates the instruments, which perform the actual surgery in the eye of the patient.

*In this report **pen** always refers to the **master** part held by the surgeon, while **instrument** always refers to the **slave** part inside the eye of the patient.*

A display near the surgeon (not depicted) shows the operation area, created by microscope or endoscope. The pens and display are attached to a coarse mechanism and can be adjusted to provide an ergonomic posture for the surgeon. In figure 2.4 a block diagram is shown, to clarify the control of the robot.

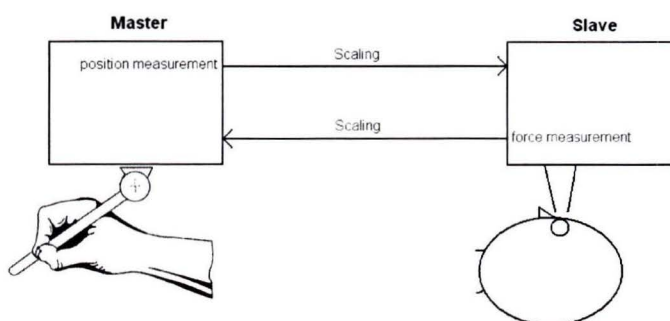


Figure 2.4: Master-slave control

The movements of the haptic pens are measured by encoders. The slave will use this position as set point and tries to reach it.

Scaling of movements can be added to obtain higher precision of the instrument movement. For example, when the surgeon is working near the retina, the scaling of the hand movement could be set to 1:100. Then, 10 mm hand movement leads to an instrument movement of only 0,1 mm. Tremor of the hand could also be eliminated by the control loop.

More than 75% of all forces occurring at vitreo-retinal surgery are below 7,5 mN. A well trained surgeon is not able to detect forces below 7,5 mN [3]. However, these forces will be measured by the slave. The master will apply the magnified forces to the hand of the surgeon. He should obtain a better 'feeling' of the instrument actions in the eye.

3 Requirements of the haptic pen

The design of the haptic pen is the subject of this report. First the requirements for the pen will be stated, based on assumptions made before this graduation project started.

3.1 Degrees of freedom

Each instrument in the eye of the patient has four degrees of freedom (DOF), as shown in figure 3.1A. In the trocar point, the instrument has a φ and ψ rotation. The instrument can rotate about its longitudinal axis, the θ rotation, and translates along this axis, the z translation. When the instrument is for example a gripper, the gripping movement will be considered the fifth DOF.

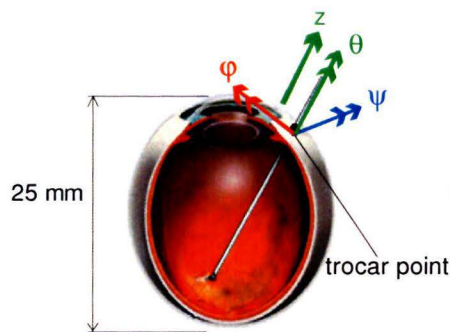


Figure 3.1A: instrument in real eye

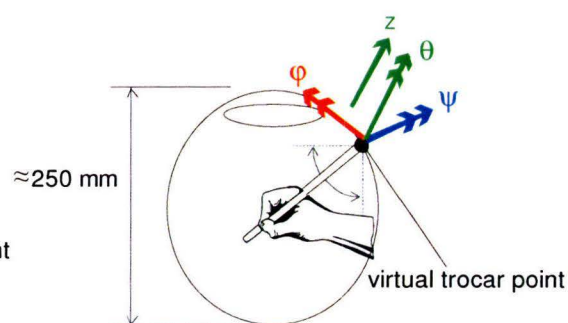


Figure 3.1B: haptic pen in virtual eye

When operating from outside, the surgeon needs to make translational steps between where he wants his instrument tip to go and where his hand should move to.

By virtually placing the hands of the surgeon within the eye of the patient a more natural way of controlling the instruments is presented. The haptic pen must have exactly the same DOF as the instrument to create a virtual trocar point (figure 3.1B). The length l of the pen, from its virtual trocar point to the place the surgeon holds it, is determined empirically to be approximately 150 mm. This length gave the most comfortable feeling while rotating in φ and ψ . With this length, a virtual eye is created, which is approximately 10 times larger than the real eye.

3.2 Ranges

In φ and ψ direction, the range of the pen is the same as its instrument. There will be a one to one scaling. Both φ and ψ have a range of $\pm 45^\circ$, limited by the lens and eye wall (figure 3.1B). The θ range of the instrument is 360° . The surgeon rolls the instrument between his fingers to obtain this range. With force feedback applied to the haptic pen, it should be held tight. Therefore, the haptic pen will be rotated in θ by rotating the wrist joint. Without re-grabbing it, the maximum stroke is $\pm 90^\circ$. To control the instrument in its whole range one could think of a jogging mode:

$$\begin{aligned}
 \theta_{pen,min} < \theta_{pen} < \theta_{pen,max} & ; & \theta_{instrument} = \theta_{pen} \\
 \theta_{pen} \geq \theta_{pen,max} & ; & \dot{\theta}_{instrument} = +C \\
 \theta_{pen} \leq \theta_{pen,min} & ; & \dot{\theta}_{instrument} = -C
 \end{aligned} \tag{3.1}$$

Where C is an adjustable constant. The total z stroke of the instrument in the eye is $\pm 12,5$ mm. Scaling proportional to the pen length leads to a z stroke of the pen of ± 75 mm. As mentioned above, a pen length of 150 mm feels nice. Therefore the z stroke should be smaller and is determined empirically to be $\pm 7,5$ mm. Again a jogging mode will be introduced. The total stroke of the button is determined to be 5 mm.

3.3 Force feedback

Because the pen should have a haptic character, all these DOF should be able to produce a force on the hand of the surgeon. Empirically, forces and torques are determined for all the DOF, based on what feels comfortable (table 3.1). The haptic pen should be able to deliver the continuous forces (F_{cont}) and torques (T_{cont}) during the whole operation, simulating general actions in the eye. The peak forces (F_{peak}) and torques (T_{peak}) simulate hard contact or possibly a virtual range limitation, both less frequently occurring situations. For these forces and torques, a duty cycle of 10% of the time is required.

The lowest force and torque change an average human can notice is approximately 7% of the applied force [4]. Therefore, the maximum friction force ($F_{f,max}$) and torque ($T_{f,max}$) should be below this percentage. In table 3.1 a summary of the five degrees of freedom with their range and force requirements is given.

Table 3.1: range and force requirements

DOF	Range	F_{cont} / T_{cont}	F_{peak} / T_{peak}	$F_{f,max} / T_{f,max}$
φ	$\pm 45^\circ$	2,5 N*	10 N*	0,2 N*
ψ	$\pm 45^\circ$	2,5 N*	10 N*	0,2 N*
θ	$\pm 90^\circ$	$30 \cdot 10^{-3} Nm$	$50 \cdot 10^{-3} Nm$	$2 \cdot 10^{-3} Nm$
z	$\pm 7,5$ mm	2,5 N	5 N	0,2 N
button	5 mm	2 N	5 N	0,2 N

* Forces sideways on the position where the surgeon holds the pen ($l \approx 150$ mm)

3.4 Resolution

The resolution of the pen is the smallest measurable movement of the pen at the position of the surgeon's hand. The value for the resolution is based on the precision with which a surgeon can position his hand. The highest resolution of the eye surgeons hand is $5 \cdot 10^{-5} m$ [3]. Therefore, the pen should have a resolution $R \leq 5 \cdot 10^{-5} m$.

3.5 Stiffness

The finite stiffness c of the pen causes an indeterminate position of the tip of the pen in two ways:

Friction causes an indeterminate position, called virtual backlash S_v given by [5]:

$$S_v = \frac{2|W|}{c} \quad (3.2)$$

With:

$$W \leq F_{f,\max}$$

$$S_v \leq R$$

Which means:

$$c \geq 8 \cdot 10^3 N / m$$

And the applied force feedback F causes deflection f of the pen without encoders noticing given by:

$$f = \frac{F}{c} \quad (3.3)$$

With:

$$f \leq R$$

$$F = F_{peak}$$

Which means:

$$c \geq 2 \cdot 10^5 N / m$$

Therefore, the pen should have a stiffness of at least $2,1 \cdot 10^5 N / m$ in all directions, felt at the position the surgeon holds the pen.

4 Haptic pen design

4.1 Pen composition

In figure 4.1 a photo is shown of the (partly assembled) right haptic pen. The left pen is an identical but mirrored version. The pen is mounted to a test frame, which is designed for testing and demonstrating purposes only.

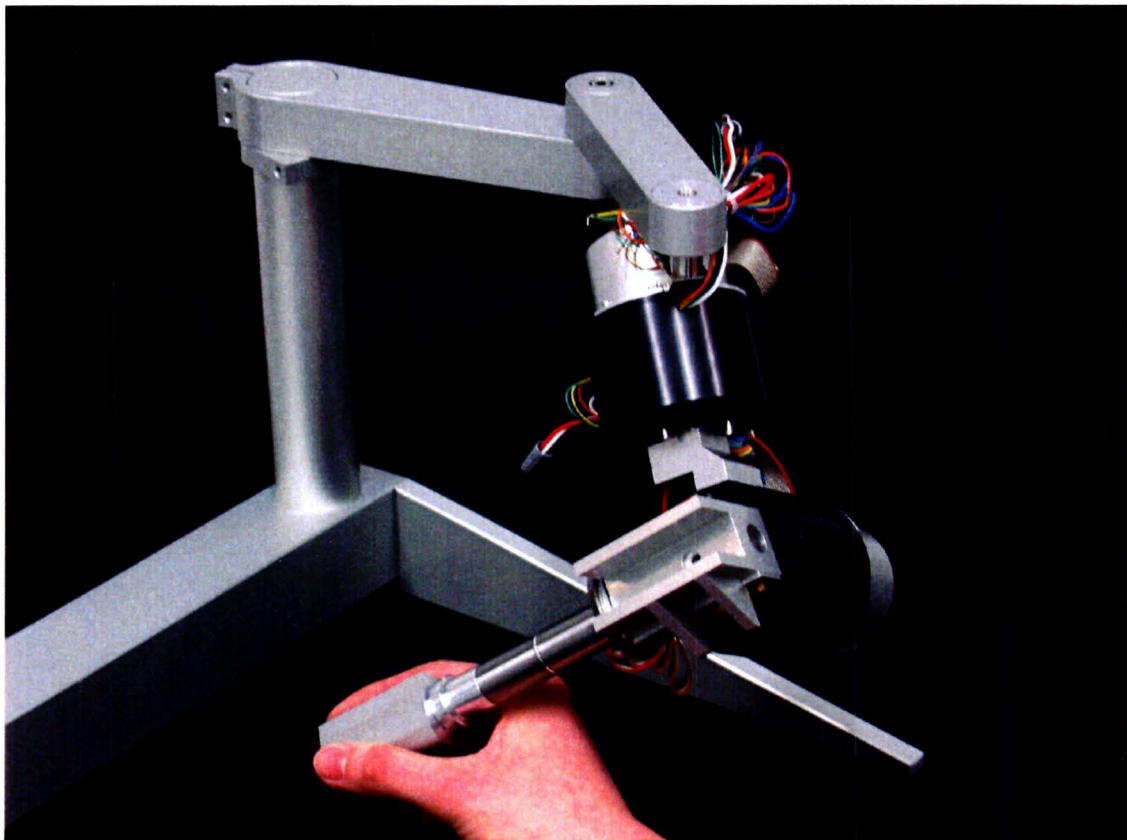


Figure 4.1: The constructed right haptic pen

This design is divided in four sub designs (figure 4.2): the φ - ψ part (red/blue), the θ -z part (green), the button part (yellow) and the weight compensation (brown).

A motor inside the φ -part drives the φ -shaft which is attached to the ψ -part which also has a motor inside. The shaft from the ψ -part is attached to the z- θ part. This part contains a bush which enables a θ -rotation and z-translation. At the downside of the bush there is a button part, which will be held by the surgeon. This part contains a button. The centerlines of the φ - and ψ -shaft and the bush intersect in point TP. Thus, a virtual trocar point is created, according to the real trocar point of the instrument in the eye of the patient (figure 3.1). The button part can be moved in the required four degrees of freedom: φ , ψ , θ and z.

The pen is suspended to the fixed world with an angle of 45° to the gravitation vector g. This to ensure the φ and ψ mid-position is consistent with the mid-position of the instrument in the eye.

A weight compensation is added to the pen, to make it statically balanced. The four sub designs will be discussed separately in the next paragraphs.

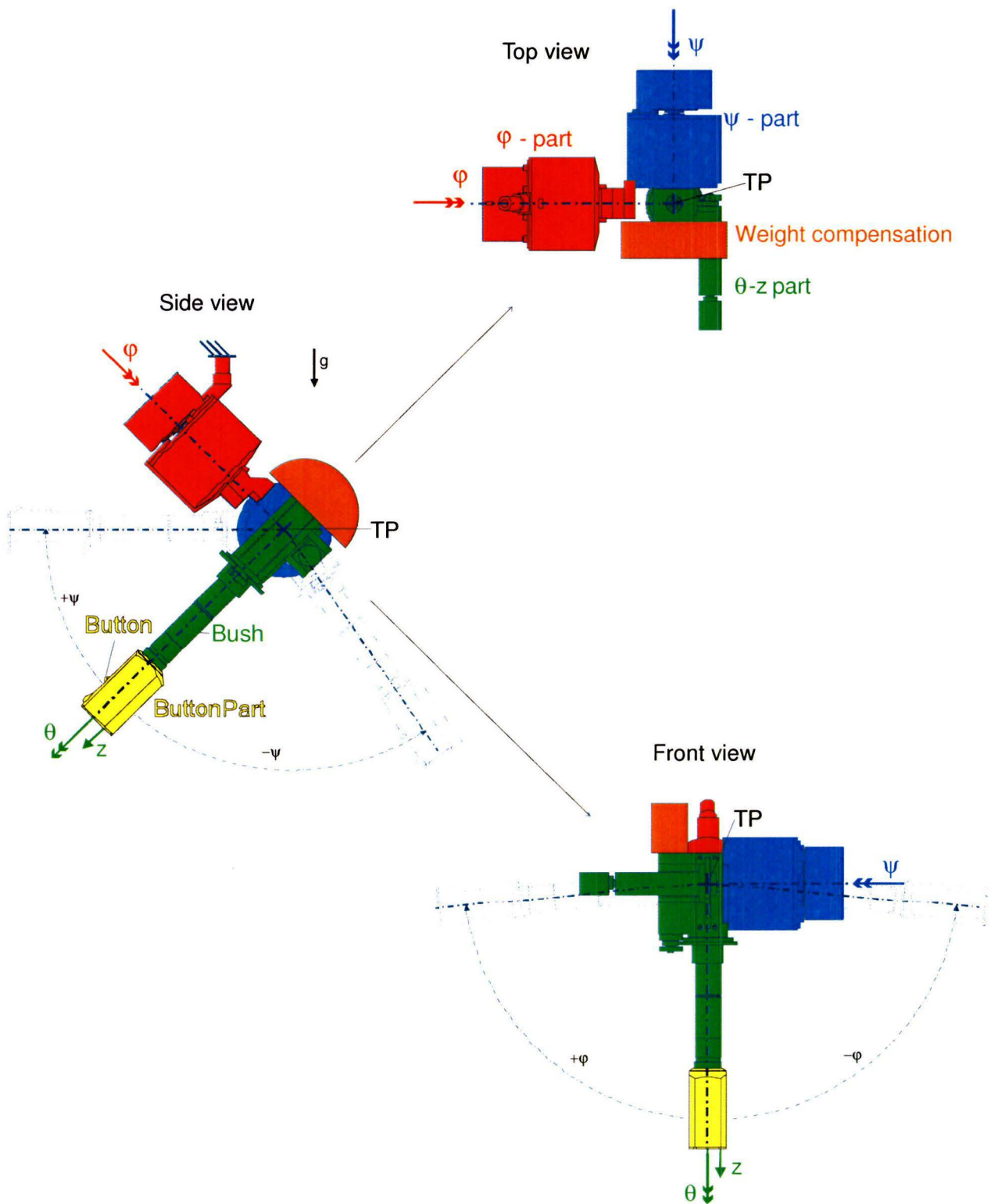


Figure 4.2: Division of the haptic pen in side, top and front view

4.2 φ and ψ part

The main difference between the φ - and ψ -part is the position where the housings are attached: the φ -housing is attached at the back side to the fixed world, while the ψ -housing is attached to the φ -shaft at its front side. Because of the resemblance of the φ - and ψ -part, the φ -part will be used to explain them both. When not explicitly indicated otherwise, the values stated for the φ -part are applicable for the ψ -part as well.

In figure 4.3 a cross section of the φ -part is shown. The main parts are labeled and will be discussed.

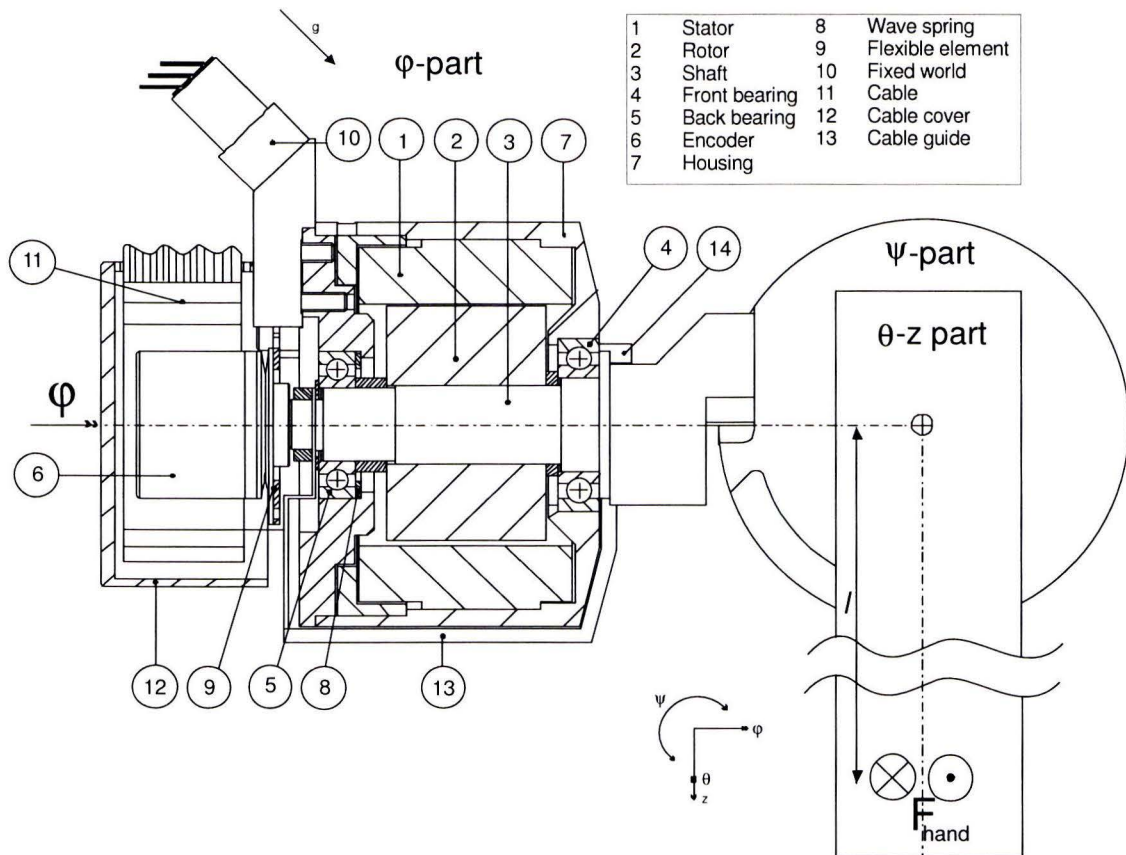


Figure 4.3: Cross-section φ part

4.2.1 Direct drive

A motor, consisting of a stator (1) and rotor (2), forms the core of the φ part. The motor drives the φ -shaft (3) by direct drive. It must be able to deliver the required force feedback (table 3.1) in φ direction to the surgeon's hand. This force F_{hand} is given by:

$$F_{hand} = \frac{T_m}{l \cdot i} \quad (4.1)$$

where the transmission ratio i is given by:

$$i = \frac{\text{outgoing movement}}{\text{ingoing movement}} = \frac{\text{hand movement}}{\text{rotor movement}} \quad (4.2)$$

The ingoing movement is the rotor rotation. The outgoing movement is the surgeon's hand rotating the shaft by moving the tip of the pen at distance l from the centre line of the φ -shaft (figure 4.3). The motor generates a torque T_m .

For force transmission $i < 1$ is favourable, because a smaller motor can be used to obtain the same force. However, the friction force F_f felt by the surgeon when he moves the tip of the pen is given by:

$$F_f = \frac{T_{f,tot}}{l \cdot i} + F_{hand} \cdot (1 - \eta) \quad (4.3)$$

where $T_{f,tot}$ is the total friction force caused by the bearings, encoder and motor. The efficiency of a transmission is given by η . The friction caused by the gear is assumed to be a percentage of the applied force feedback F_{hand} . For gear transmission η is approximately 0,98 [4]. The felt friction force is increased when i is decreased. A trade off is made between friction force and motor compactness. Using no transmission at all:

$$i = 1 \text{ and } \eta = 1.$$

An advantage of direct drive is that extra measures to eliminate the backlash in the transmission can be omitted. Backlash causes position uncertainty of the pen when changing direction. The resolution of the pen is directly lowered by the size of it. The resolution will be discussed in paragraph 4.2.4.

In the next paragraph the motor choice will be discussed and it will be shown that direct drive will meet the required feedback forces and maximum friction forces.

4.2.2 Motor choice

Brush motors generate a torque ripple that is a percentage of their produced torque, typically a few percent. Added to this ripple there is an unpredictable torque, caused by the brushes. Control cannot cancel it out. As mentioned in the requirements, a human can feel force deviations of approximately 7%. The unpredictable torque could be higher than this percentage. Therefore, brush motors will not meet the requirements. Brushless motors also generate a torque ripple, when using block commutation. This ripple is typically 14% of the produced torque. Using sinusoidal commutation, the ripple can be eliminated. Iron based brushless motors with the highest torque density (torque to volume ratio) generate cogging. This is a torque disturbance based on the magnets in the field attraction to the teeth in the armature. It is a predictable torque ripple $T_{f,ripple}$ that is independent of the produced torque. The motor also generates a static friction torque $T_{f,static}$.

The front (4) and back (5) deep groove ball bearings generate a friction torque $T_{f,b}$ (calculation in appendix B). The encoder (6), mounted on the back of the shaft, has ball bearings inside, also generating a friction torque $T_{f,e}$ (datasheet in appendix A).

The total friction torque in φ from (4.3) is given by:

$$T_{f,tot} = T_{f,ripple} + T_{f,static} + T_{f,b} + T_{f,e} \quad (4.4)$$

The brushless Kollmorgen RBE 01512 motor with sinusoidal commutation (datasheet in appendix A) in direct drive meets the requirements with (4.1) and (4.3):

$$\begin{aligned} T_{m,cont} &= 0,5 Nm \\ T_{m,peak} &= 1,7 Nm \\ T_{f,static} &= 1,7 \cdot 10^{-2} Nm \\ T_{f,ripple} = T_{cogging} &= 1 \cdot 10^{-2} Nm \\ T_{f,b} &= 3 \cdot 10^{-4} Nm \\ T_{f,e} &= 5 \cdot 10^{-3} Nm \\ l &= 1,5 \cdot 10^{-1} m \end{aligned}$$

Required:	Obtained with this motor:
$F_{cont} = 2,5 N$	$F_{cont} = 3 N$
$F_{peak} = 10 N$	$F_{peak} = 11 N$
$F_{f,max} = 0,2 N$	$F_f = 0,2 N$

In the ψ part, only the friction torque of the bearings is a factor 3 lower, because of the smaller load on it. Therefore, it also meets the requirements.

4.2.3 Bearing stiffness and load

The motor is frameless. Therefore, a compact housing (7) is designed around the motor. The radial stiffness of the ball bearings that connect the rotating φ -shaft and the fixed housing is the critical stiffness of the φ -part (in appendix C stiffness of all parts is determined, even after optimizing the bearing stiffness it is one of the weakest links). Larger bearings have higher stiffness c and load capacity C_0 [7] and [8], but also higher friction torque. A bearing generates a friction torque given by (calculation in appendix B):

$$T_{f,b} = \mu \cdot F \cdot \frac{d_m}{2} \quad (4.5)$$

where F is the radial load on the bearing and d_m the mean bearing diameter. In figure 4.4 a simplified model of the φ -shaft held by two deep groove ball bearings with stiffness c_1 and c_2 is shown.

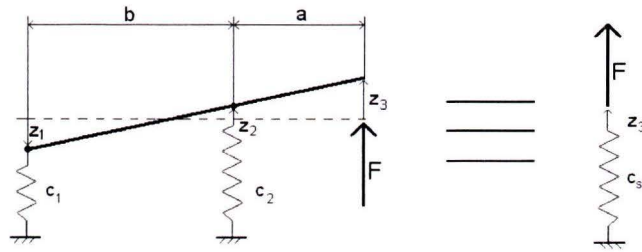


Figure 4.4: substitute bearing stiffness

The force F (generated for example when force feedback in z direction is applied) is perpendicular to the centerline of the pen and works from outside the two bearings. The substitute radial stiffness c_s is given by (appendix C):

$$\frac{1}{c_s} = \frac{\left(\frac{a}{b}\right)^2}{c_1} + \frac{\left(\frac{a+b}{b}\right)^2}{c_2} \quad (4.6)$$

To obtain the highest substitute stiffness, the distance b between the front and back bearing has been maximized within the housing, while the distance a from the front bearing to the pen centre line is minimized. This has been realized by an O-arrangement as can be seen in the dotted line in figure 4.5. The dotted line is the simplified force loop.

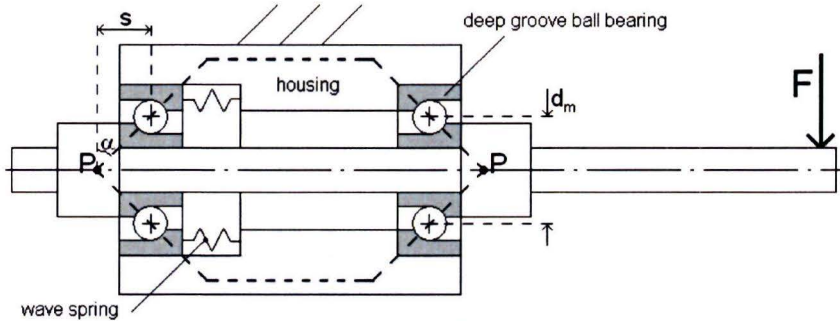


Figure 4.5: Bearing O-arrangement

The deep groove ball bearings are pretensioned by a wave spring ((8) in figure 4.3). The bearing pole P is placed outside the housing with a distance s given by:

$$s = \frac{d_m}{2} \tan \alpha \quad (4.7)$$

where α is the pressure angle for the bearing chosen. The deep groove bearings can then be seen as angular contact bearings. Pretensioning of the bearings also cancels out play and increases the stiffness of the bearing pair [7]. The axial preload should exceed the maximum axial load of 10 N to make sure the shaft will always make axial contact with both bearings. This maximum load occurs when the maximum ψ force feedback of 10 N is applied.

The distance a and b from (4.6) are now given by a' and b' :

$$a' = a - s \quad (4.8)$$

$$b' = b + 2 \cdot s \quad (4.9)$$

With:

$$\alpha = 20^\circ$$

$$d_m = 20 \cdot 10^{-3} \text{ m}$$

$$a = 56 \cdot 10^{-3} \text{ m}$$

$$b = 39 \cdot 10^{-3} \text{ m}$$

$$c_1 = c_2 = 6 \cdot 10^6 \text{ N / m}$$

$$\Rightarrow c_s = 7 \cdot 10^5 \text{ N / m}$$

This meets the stiffness requirement of 3.3, p.9. In the ψ part, the bearing stiffness will be even higher because a and b are given by:

$$a = 12 \cdot 10^{-3} \text{ m}$$

$$b = 42 \cdot 10^{-3} \text{ m}$$

$$\Rightarrow c_s = 3 \cdot 10^6 \text{ N / m}$$

The maximum load capacity of each bearing is approximately 2000 N, while the maximum axial load is approximately 25 N (appendix C) and the radial load 20 N (feedback force plus pretension). The bearing load capacity is sufficient.

In paragraph 4.6 an overview of the stiffness of all components of the φ and ψ parts in all directions will be given.

4.2.4 Resolution

At the backside of the shaft a Scancon 2RMHF encoder ((6) in figure 4.3 p.14) is placed to measure the angular displacement (datasheet in appendix A). The encoder consists of a fixed housing and a hollow shaft attached to the shaft (figure 4.6). It has an internal bearing pair and thereby five degrees of freedom are constrained for the housing. A flexible element (9) is used to constrain the only free DOF: the φ -rotation, without over-constraining the other DOF.

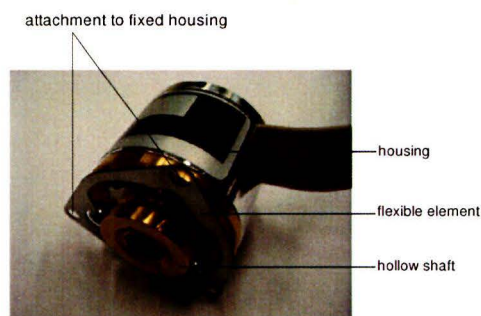


Figure 4.6: encoder with flexible element

The encoder generates 30000 counts per turn (*cpt*). The resolution R in φ direction at the surgeon's hand is given by:

$$R_{\varphi} = \frac{2\pi \cdot l}{cpt \cdot i} \quad (4.10)$$

$$\Rightarrow R_{\varphi} = 30 \cdot 10^{-6} m$$

This is less than the maximum required resolution $R \leq 5 \cdot 10^{-5} m$, the encoder meets the requirements. However, virtual backlash adds up to R_{φ} . In paragraph 4.6 the virtual backlash will be determined, and it will be shown that the overall resolution requirement will be met.

4.2.5 Cable

Motors and encoders in the ψ , θ -z and button parts are electronically connected to the fixed world (10) with two flat flexible cables (11). To make the transition for the cables between the rotating part and fixed part without generating high and unpredictable disturbance forces, the cables are spirally wrapped around the encoder. One end is attached to a fixed cable cover (12), while the other end is rotating along with the φ -shaft. To guide the cables into the cover and to make sure they rotate along with the shaft, the cables are strapped to a cable guide (13). This guide is attached to the front and back end of the shaft. The cables can be considered to be a spiral spring. In appendix D the flexible flat cable is explained and its maximum spring torque is determined. When the φ -shaft is in its extreme position, the cable generates a force on the surgeon's hand of

$$F_{cable} = 7 \cdot 10^{-3} N .$$

This is lower than the noticeable force deviation of 7% of the feedback force. Furthermore, this force is proportional to the φ rotation and therefore with feed forward it can be compensated for by the motor.

At the back of the ψ house the cable from the θ -z and button part is coiled up. The disturbance force in ψ is even smaller, because a smaller cable for these two parts is coiled more easily.

4.2.6 Range

The required range in φ is $\pm 45^\circ$. However, the mechanical design does not limit the rotation (figure 4.2: front view, p.13). The cable windings are designed to make a rotation of $\pm 90^\circ$. Two end stops (14) mechanically limit this range, to prevent the cables from being damaged. Later on testing of the pen will show if this extra stroke has any benefits or can be reduced further.

The required range in ψ is also $\pm 45^\circ$. The mechanical design limits the pen in $+45^\circ$ and -270° . Larger stroke will lead to a collision between the θ -z part and the φ -part (figure 4.2: side view, p.13). Making a stroke of -90° leads to coinciding of the centre line of the φ - and θ -rotation. The system becomes singular: one degree of freedom can be actuated by two actuators. To prevent indifferent behavior, cable damage and collision between the θ -z and φ -part, two end stops limit the range to $+45^\circ$ and -88° .

4.3 θ -z part

In figure 4.7 a cross section of the θ -z part is shown. The main parts are labeled and will be discussed.

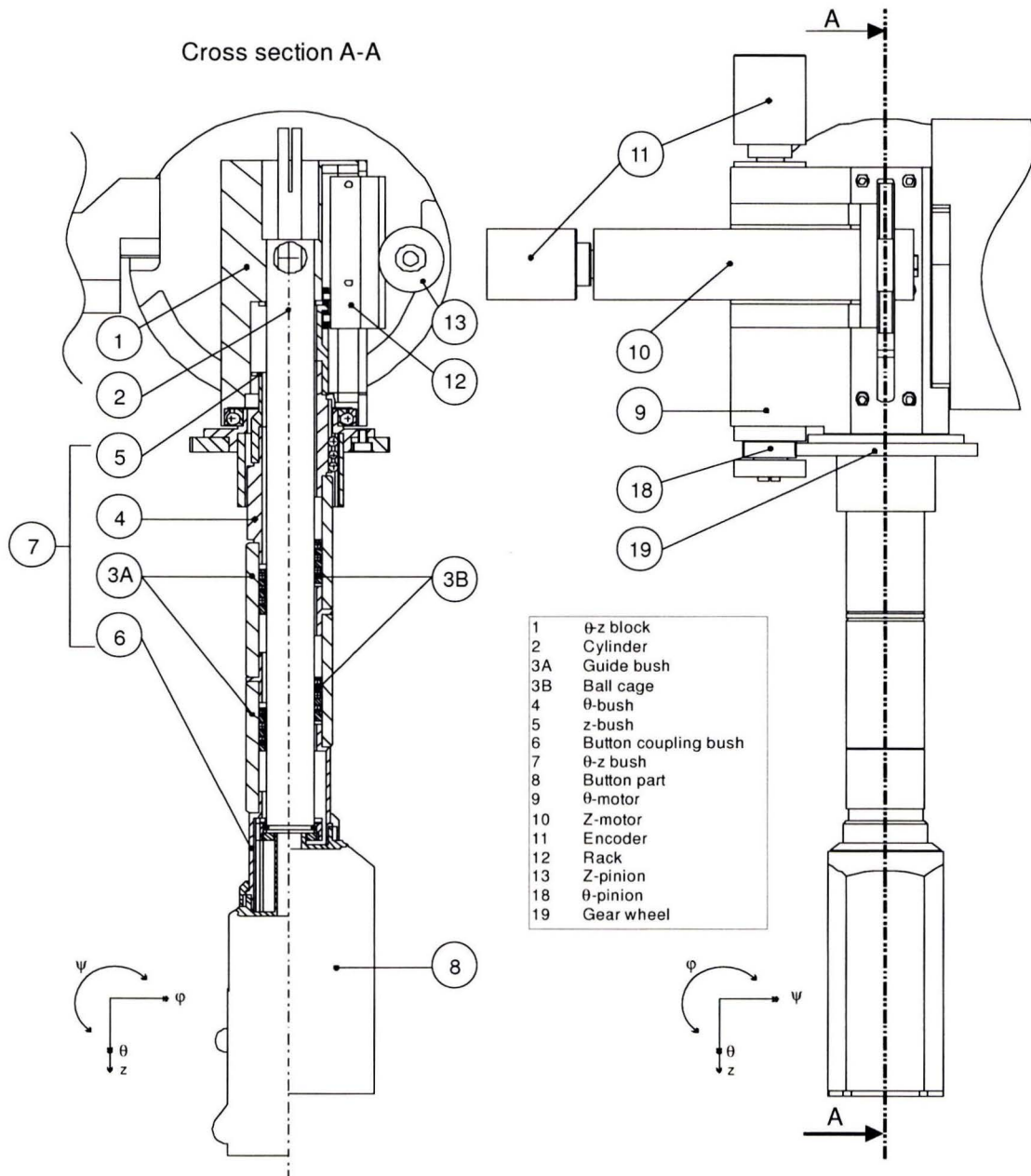


Figure 4.7: cross-section of the θ -z part

The θ -z block (1) and cylinder (2) attached to it, form the base for the θ -z part. These parts can only move in ϕ and ψ direction. Over the cylinder, two rotation- translation bearings are placed, each consisting of a guide bush (3A) and ball cage (3B) (see also figure 4.8).

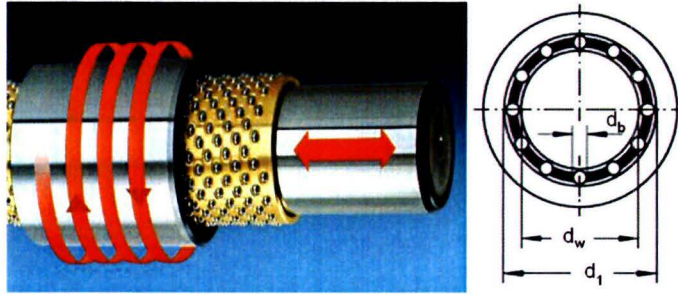


Figure 4.8: rotation/translation bearing

Together with the θ -bush (4), z-bush (5) and button coupling bush (6), they form the θ -z bush (7). The button part, which is held by the surgeon, is attached to this bush. The bearings make a combined θ and z movement possible for the bush and button part (8).

4.3.1 Parallel θ -z drive

The θ -z bush is provided with parallel θ and z force feedback. The θ -motor (9) and z-motor (10) are attached to the θ -z block. To make the parallel θ -z drive possible, the z-drive must be uncoupled from the θ movement, while the θ -drive must be uncoupled from the z movement, as will be discussed in paragraph 4.3.3.4 and 4.3.4.4 respectively.

The moving mass in θ and z direction is lowered by this parallel drive. The gravitational force on all the moving masses is a disturbance force. In z direction, compensating for that mechanically is difficult. Lower moving mass in z results in lower disturbance force in this direction. In paragraph 4.5, weight compensation will be discussed further. Another advantage of the parallel drive is no disturbance forces in θ and z are generated by cables of the motors and encoders (11).

4.3.2 Motor choice

The volume available for the θ and z drive is not sufficient to use direct drive feedback. Therefore a reduction $i < 1$ has been chosen. Therby, smaller motors can be used, for the same force feedback. The disturbance forces felt by the surgeon caused by the inertia of the moving rotor is given by:

$$F_{inertia} \propto \frac{1}{i^2} \quad (4.11)$$

$$F_{inertia} \propto J_{rotor} \quad (4.12)$$

where J_{rotor} is the rotor inertia. A motor is chosen based on highest nominal torque, weighting quadratic (according to 4.11), and lowest rotor inertia, weighting linear (according to 4.12). The Maxon EC 16 brushless motor (appendix A) is chosen to drive θ and z.

4.3.3 Z-drive

In figure 4.9 the z drive is shown separated from the rest of the θ z part.

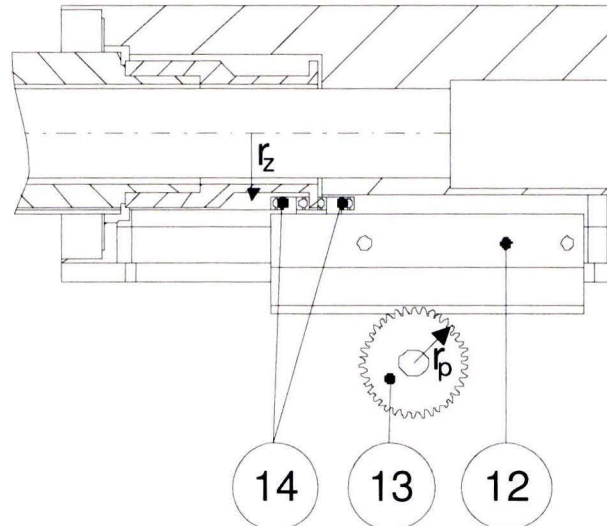


Figure 4.9: z-drive

4.3.3.1 Z-transmission

The z drive uses a rack (12) and pinion (13) transmission. The z force feedback is given by:

$$F_{hand} = \frac{T_m}{i_z} \quad (4.13)$$

The ratio is given by the pitch radius of the pinion r_p by:

$$i_z = r_p \quad (4.14)$$

With:

$$\begin{aligned} r_p &= 5,7 \cdot 10^{-3} \text{ m} \\ T_{m,cont} &= 13,9 \cdot 10^{-3} \text{ Nm} \\ T_{m,peak} &= T_{stall} = 184 \cdot 10^{-3} \text{ Nm} \end{aligned}$$

Required:

$$\begin{aligned} F_{cont} &= 2,5 \text{ N} \\ F_{peak} &= 5 \text{ N} \end{aligned}$$

Obtained with this motor:

$$\begin{aligned} F_{cont} &= 2,4 \text{ N} \\ F_{peak} &= 32 \text{ N} \end{aligned}$$

4.3.3.2 Anti backlash gear

The pinion is an anti backlash gearwheel, to eliminate backlash appearing when the motor torque direction is switched (figure 4.10).



Figure 4.10: anti backlash gearwheel

It consists of two concentric gears. The carrying wheel is attached to the motor shaft. The other wheel is preloaded with respect to the carrying wheel by a wound up wire C-spring. In both driving directions, both gears mesh with the rack. To do so, the pretension should exceed the maximum force applied. Therefore the minimum preload torque of the spring should be:

$$T_{preload} = F_{peak, min} \cdot r_p \quad (4.15)$$

$$\Rightarrow T_{preload} = 29 \cdot 10^{-3} Nm$$

The supplier is able to deliver springs that can create $T_{preload} = 17,5 \cdot 10^{-3} Nm$. This is not sufficient, and therefore the spring should be replaced. The torsional stiffness of a C-spring is given by[9]:

$$k_b = \frac{\pi E d^4}{l} \quad (4.16)$$

where E is the modulus of elasticity, d the diameter and l the length. A diameter increase of factor $\sqrt[4]{1,6} = 1,1$ gives the required pretension in the spring. The highest allowable stress σ_{max} is given by:

$$\sigma_{max} = \frac{32T_{max}}{\pi d^3} \quad (4.17)$$

resulting in a stress increase of factor 1,5 with the given torque increase and diameter increase. A spring material with this factor higher σ_{max} must prevent it from failing with the new pretension.

The total gear efficiency for the anti backlash gear transmission is approximated by using the efficiency of a one step transmission ($\eta = 0,98$ from [4]) for each preloaded gear half, resulting in:

$$\eta = 0,98^2 = 0,96$$

The maximum friction force in z generated by the transmission $F_{f,gear}$ is given by:

$$\begin{aligned} F_{f,gear} &= F_{hand} \cdot (1 - \eta) \\ \Rightarrow F_{f,gear} &= 0,1N \end{aligned} \quad (4.18)$$

This is 50% of the maximum allowable z friction. In paragraph 4.3.5 the total friction felt in z is discussed.

4.3.3.3 Tooth strength

The gear module m is taken as small as possible (determined by supplier), to obtain the smoothest gear meshing. In appendix E gear strength based on tooth root strength (F_{ts}) and tooth flank pitting (F_{tw}) is calculated, where the pinion is the weakest link. The maximum tangential force on the pinion at which it can operate indefinitely (pinion revolutions $>10^7$) is given by:

$$\begin{aligned} F_{ts} &= 14N \\ F_{tw} &= 4,5N \end{aligned}$$

The tooth pitting force is less than F_{peak} . This peak force is only applied with a maximum of 10% of the time. Therefore, tooth wear is assumed to be negligible and the gear will be sufficient. However, when testing shows otherwise, the gear material can be changed from Stainless steel 303 to hardened stainless steel 17-4PH. Then, $F_{tw} = 30N$.

4.3.3.4 θ -uncoupling

The translating rack drives the z bush (5) in z direction by two miniature roller bearings (rollers) (14) (figure 4.9). The rollers allow the bush to rotate freely in θ . The rim between the rollers is approximately 5 μm larger than the neutral distance between the rollers. This causes a light preload (5 N) of the rollers, eliminating clearance and increase of radial stiffness. Stiffness in z direction of each roller is approximately $c_z = 2 \cdot 10^6 N / m$ (appendix C). The static load capacity of each roller is 30 N, while the maximum load and pretension together is 10 N.

To obtain the lowest moment on the bush, the driving force should be applied as close as possible to its center line. The rollers apply the z force at $r_z = 7$ mm from the bush center line, creating a moment on the bush (figure 4.9). From equilibrium of force and moment, the maximum extra load on the rotation/translation bearings is 20% of the applied z force. This is a very small load compared to the load on the bearings caused by a ϕ or ψ force as will be explained in the next paragraph.

4.3.3.5 Rotation/translation bearing stiffness and load

When applying a ϕ or ψ force to the hand of the surgeon, the bearings will be loaded similar overhung to the bearing pair in the ϕ and ψ house (figure 4.4, p17). The distance b between these bearings should be as large as possible while the distance a between the position where the surgeon holds the pen and the first bearing should be as small as possible, to obtain the highest radial stiffness and lowest maximum load P_{max} on the bearings.

The radial stiffness c of the bushes is approximated by comparing the radial static loading capacity C_0 of the bushes with that of a deep groove ball bearing (appendix C). From (4.6) on p.17 with:

$$\begin{aligned}
 F_\phi &= 10N \\
 a &= 60 \cdot 10^{-3} m \\
 b &= 30 \cdot 10^{-3} m \\
 C_0 &= 60N \\
 \Rightarrow P_{\max} &= 31N \\
 c &= 5 \cdot 10^6 N / m \\
 \Rightarrow c_s &= 5 \cdot 10^5 N / m
 \end{aligned}$$

The stiffness as well as the loading capacity of the bearings is sufficient.

The bearings are pretensioned to eliminate clearance. High pretension gives higher radial stiffness and higher friction. The stiffness meets the requirement, therefore the lightest pretension advised by the producer is chosen, to obtain the lowest friction (in paragraph 4.3.5 the friction in θ and z will be discussed). The pretension is accomplished by a diameter difference $\Delta d = 3 \cdot 10^{-6} m$ between the shaft diameter d_w and bush inner diameter d_1 given by:

$$\Delta d = d_w + 2 \cdot d_b - d_1 \quad (4.19)$$

where d_b is the ball diameter, see figure 4.8, p.21. There is a load reserve of approximately 100%. If testing of the guiding shows an unsatisfactory friction level, up to 50% of the balls can be removed to lower it.

4.3.3.6 Rack guiding

The forces acting on the rack (12) are shown in figure 4.11A. The tooth force vector, created by the pinion (13), makes an angle of 20° with the z direction. To keep the rack in place, it is guided by four guiding rollers (15) on two running surfaces (16). These running surfaces are on opposite sides of the rollers, because F_1 and F_2 also act in opposite direction. The two upper rollers run over the guiding plate (17), while the two lower rollers run over the θ - z block (1). The z force is transmitted to the bush by the z -rollers (14).

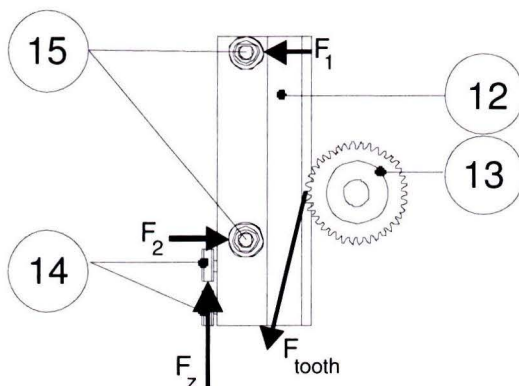


Figure 4.11A: side view rack

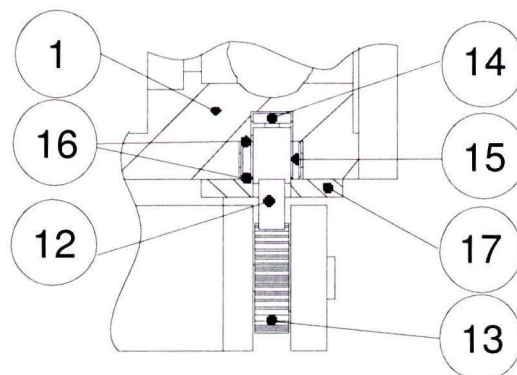


Figure 4.11B: top view rack

In figure 4.12 a photograph is shown of the manufactured rack guiding.

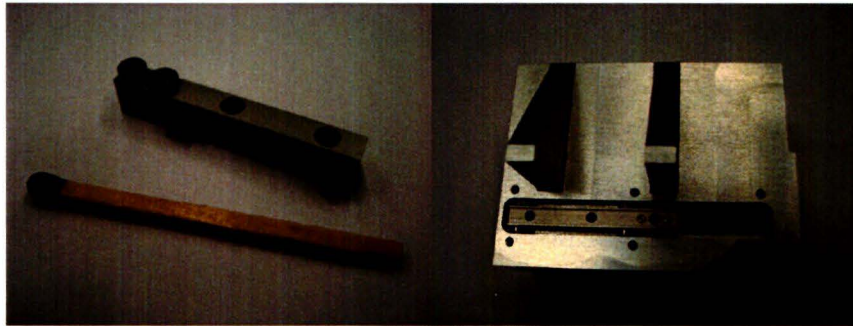


Figure 4.12: rack guiding

4.3.3.7 Z-Resolution

At the back of the motor, an encoder ((11) in figure 4.7 on p.20) with 20000 counts per turn is placed (datasheet in appendix A). With (4.10) from p.19:

$$l = r_p$$

$$\Rightarrow R_z = 1,8 \cdot 10^{-6} m$$

This is much less than the maximum required resolution of $R \leq 5 \cdot 10^{-5} m$, therefore this encoder meets the requirement. However, virtual backlash adds up to R_z . In paragraph 4.6 the virtual backlash will be determined, and it will be shown that the overall resolution requirement will be met.

4.3.3.8 Z-Range

The extreme positions in z are shown in figure 4.7. A z stroke of ± 8 mm is possible. At the two z end-stops rubber rings are added, to lower the collision force F_c , given by:

$$F_c = v_c \sqrt{m \cdot c} \quad (4.20)$$

where v_c is the collision velocity. The stiffness of a ring is proportional to its Young's modulus E , which for rubber is approximated by $E_{rubber} = 5 \cdot 10^6 N / m^2$, a factor 40000 lower than steel [10].

4.3.4 θ -movement

4.3.4.1 θ -Transmission

The θ drive also uses a Maxon EC 16 brushless motor. A one step gear transmission is used (pinion (18) and wheel (19) in figure 4.7 on p.20). The θ torque feedback to the hand is given by:

$$T_{hand} = \frac{T_m}{i_\theta} \quad (4.21)$$

The ratio i is given by the pitch radius of the pinion (r_p) and wheel (r_w) according to:

$$i_\theta = \frac{r_p}{r_w} \quad (4.22)$$

$$r_w = 20,25 \cdot 10^{-3} m$$

$$r_p = 5,7 \cdot 10^{-3} m$$

Required:

$$T_{cont} = 30 \cdot 10^{-3} Nm$$

$$T_{peak} = 50 \cdot 10^{-3} Nm$$

Obtained:

$$T_{cont} = 49 \cdot 10^{-3} Nm$$

$$T_{peak} = 650 \cdot 10^{-3} Nm$$

4.3.4.2 Anti backlash gear

The θ pinion is also an anti backlash gearwheel. The pretension torque should exceed the maximum torque applied on the pinion:

$$T_{preload} = T_{peak, min} \cdot i_\theta \quad (4.23)$$

$$\Rightarrow T_{preload} = 14 \cdot 10^{-3} Nm$$

This can be delivered by the supplier.

Similar to the z drive, the total gear efficiency for the anti backlash gear transmission is approximated by using the efficiency of a one step transmission for each gear half, resulting in $\eta = 0,96$. The maximum friction torque in θ generated by the transmission $T_{f, gear}$ is given by:

$$T_{f, gear} = T_{hand} \cdot (1 - \eta) \quad (4.24)$$

$$\Rightarrow T_{f, gear} = 1 \cdot 10^{-3} Nm$$

This is 50% of the maximum allowable θ friction. In paragraph 4.3.5 the total friction felt in θ is discussed.

4.3.4.3 Tooth strength

The tooth modulus is determined similar to the z transmission. The gear strength is calculated in appendix E. This gives:

$$T_{ts} = 86 \cdot 10^{-3} \text{ Nm}$$

$$T_{tw} = 29 \cdot 10^{-3} \text{ Nm}$$

Similar to the z transmission, pitting can occur during peak load. Using hardened stainless steel 17-4PH, $T_{tw} = 190 \cdot 10^{-3} \text{ Nm}$ and no pitting should occur.

4.3.4.4 Z-uncoupling

To transfer torque to the θ bush (4) and thereby the θ -z bush, while allowing the bush to move in z direction, three ball grooves (20) are used (figure 4.13).

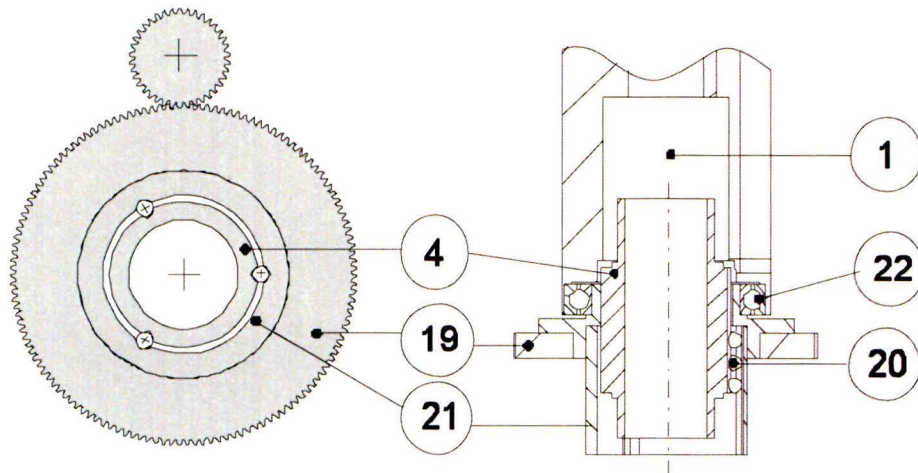


Figure 4.13: θ ball groove

The outer ring(21) with gearwheel(19) attached to it is attached to the θ -z block(1) by a deep groove ball bearing(22), to fixate it in z direction, while allowing the θ rotation. In each axial groove there are 3 balls. To eliminate play these balls are pretensioned by trying to making the groove distance $1 \mu\text{m}$ smaller than the ball diameter d_b . The ball diameters have a tolerance of $0,5 \mu\text{m}$. The groove is made by wire EDM, which has maximum precision of approximately $1 \mu\text{m}$. By trial and error, a couple of grooves have been made, to obtain a clearance free z uncoupling, with low friction. The rotational stiffness of the 3 grooves with 9 balls, is approximated to be (appendix C):

$$c_{\theta} = 2 \cdot 10^3 \text{ Nm / rad}$$

This stiffness is sufficient. However, confirmation of this still has to be done by testing this part.

4.3.4.5 θ -Resolution

At the back of the motor, an encoder with 20000 counts per turn is placed. With a grip diameter d_g where the surgeon holds the pen, the resolution is given by:

$$R_\theta = \frac{\pi \cdot d_g}{cpt \cdot i_\theta} \quad (4.25)$$

$$\Rightarrow R_\theta = 11 \cdot 10^{-6} m$$

This is less than the maximum required resolution of $R \leq 5 \cdot 10^{-5} m$, therefore this encoder meets the requirement. However, virtual backlash adds up to R_θ . In paragraph 4.6 the virtual backlash will be determined, and it will be shown that the overall resolution requirement will be met.

4.3.4.6 θ -Range

The θ rotation is limited to approximately $\pm 175^\circ$. In figure 4.14 the θ end-stop is shown. This is a simplified cross section of the coupling bush (6) and the cylinder (2) from figure 4.7, p.20.

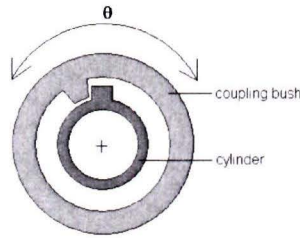


Figure 4.14: θ end-stop

4.3.5 Friction in θ and z

The friction in z is created by the 2 rotation/translation bearings, the 3 axial ball grooves, rack guiding, gear meshing, motor bearings, encoder and cable wrapping (the latter will be discussed in paragraph 4.4 and is calculated in appendix D). The highest approximated disturbance force in z is given by (appendix B):

$$F_{f,z} = F_{f,rot} + F_{f,groove} + F_{f,rack} + F_{f,gear} + \frac{1}{i_z} \cdot (T_{f,m} + T_{f,e}) + F_{cable,z} \quad (4.26)$$

With:

$$\begin{aligned}
 F_{f, tr/rot} &= 0,1N \\
 F_{f, groove} &= 0,05N \\
 F_{rack} &= 8 \cdot 10^{-3} N \\
 F_{f, gear} &= 0,1N \\
 T_{f, m+e} &= 7 \cdot 10^{-5} Nm \\
 F_{cable, z} &= 0,1N \\
 \Rightarrow F_{f, z} &= 0,4N
 \end{aligned}$$

This is more than the required maximum disturbance force of 0,2 N. However, the calculated friction force in z is a worst case approximation. Furthermore, the cable disturbance is linear with the z stroke, and therefore with feed forward it could be canceled out. Testing of the pen will show if the design should be adapted.

The friction in θ is created by the 2 rotation/translation bearings, z-rollers, gear meshing, motor bearings, encoder and cable wrapping. The highest approximated friction torque in θ is given by (appendix B):

$$T_{f, \theta} = T_{f, tr/rot} + T_{f, z-rolls} + T_{f, gear} + \frac{1}{i_{\theta}} \cdot (T_{f, m} + T_{f, e}) + T_{f, cable} \quad (4.27)$$

$$\begin{aligned}
 T_{f, tr/rot} &= 6 \cdot 10^{-4} Nm \\
 T_{f, z-rolls} &= 2 \cdot 10^{-4} Nm \\
 T_{f, gear} &= 1 \cdot 10^{-3} Nm \\
 T_{f, m+e} &= 7 \cdot 10^{-5} Nm \\
 T_{cable, \theta} &= 1 \cdot 10^{-3} Nm \\
 \Rightarrow T_{f, \theta} &= 3 \cdot 10^{-3} Nm
 \end{aligned}$$

This is more than the required maximum disturbance torque of $2 \cdot 10^{-3} Nm$. However, the calculated friction torque in θ is a coarse approximation. Furthermore, the cable disturbance is linear with the θ rotation, and therefore with feed forward it could be canceled out. Testing of the pen will show if the design should be adapted.

4.4 Button Part

The button part is held by the surgeon, in a way similar to the way an ordinary pen is held. He uses the thumb and middle finger to grab it and his index finger to operate a button (1) (figure 4.15).

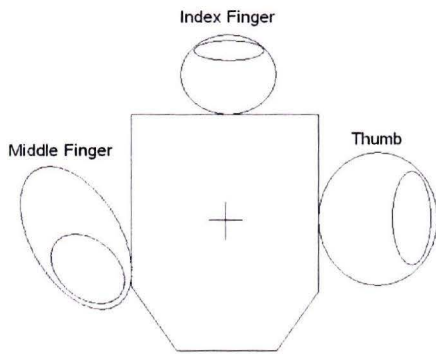


Figure 4.15A: front view of button

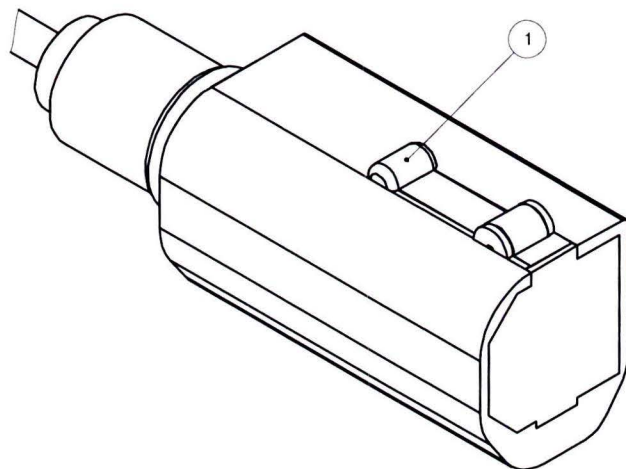


Figure 4.15B: isometric view of button

The force feedback in ϕ , ψ , θ and z direction must be transferred to the hand by these two fingers. Two (more or less parallel) surfaces are offered to the fingers, with which the surgeon grips the pen.

The button moves along with the hand in ϕ , ψ , θ and z . Therefore, the index finger is always in reach of the button.

With the button, the surgeon controls a gripping movement of the instrument in the eye of the patient. Button force feedback gives him information about the force of gripping.

The volume of the button part has to be small enough to fit nicely in between the fingers of the surgeon. A cross section of the button part is shown in figure 4.16.

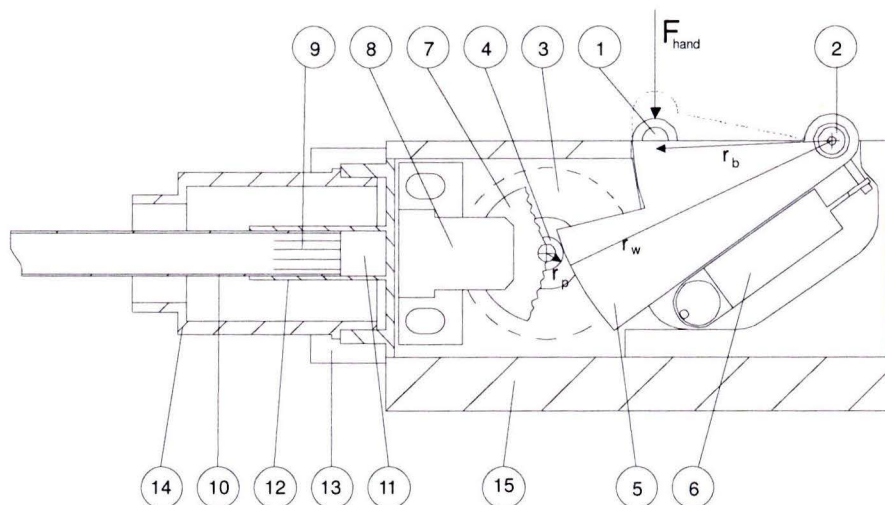


Figure 4.16: Button cross section

The button (1) should have a more or less linear movement, perpendicular to the pen centerline in its stroke of $5 \cdot 10^{-3} m$. This is the natural movement the index finger makes when pressing a button. The easiest way to fix 5 DOF of the button, while the one free DOF is the force feedback direction, is using a pivoting point. This has been made by a fixed shaft with two deep groove ball bearings (2) on it. The button stroke is then an arc. To make this a more or less linear movement, r_b should not be too small and the line between pivoting point and pressing point should be more or less parallel with the pen centre line as can be seen in figure 4.16.

4.4.1 Drive

The force feedback is generated by a small motor (3). From equation 4.13 a smaller i leads to a smaller T_m and thereby smaller motor. However, smaller i also leads to a larger transmission (or extra transmission steps), higher friction and higher inertia disturbance force given by:

$$F_{disturb} = F_{inertia} + F_f \quad (4.28)$$

With:

$$F_{inertia} = \frac{\ddot{\alpha}_b}{r_b} \cdot \left(\frac{J_m}{i^2} + J_b \right) \quad (4.29)$$

$$F_f = \frac{T_{f,b}}{r_b} + \frac{T_{f,m}}{r_b \cdot i} + F_{hand} \cdot (1 - \eta) \quad (4.30)$$

where J_m and J_b are the inertia of the rotor and button respectively. The friction torque generated by the button bearings and motor bearings is given by $T_{f,b}$ and $T_{f,m}$ respectively (appendix B). The pressing movement is assumed to be 1 Hz maximum, leading to an angular button acceleration $\ddot{\alpha}_b = 0,67 rad / s^2$ (calculation in appendix F).

The brushless Maxon EC 20 flat motor (appendix A) with a one step transmission meets the requirements. On the motor shaft a pinion (4) is mounted, driving a gear segment (5) which is attached to the button. The button force feedback is given by (i is given by 4.22 on p.27):

$$F_{hand} = \frac{T_m}{r_b \cdot i} \quad (4.31)$$

With:

$$T_{m,cont} = 3,9 \cdot 10^{-3} Nm$$

$$T_{m,peak} = T_{stall} = 8 \cdot 10^{-3} Nm$$

$$J_m = 3,8 \cdot 10^{-7} Kgm^2$$

$$r_p = 1,75 \cdot 10^{-3} m$$

$$r_w = 32 \cdot 10^{-3} m$$

$$r_b = 20 \cdot 10^{-3} m$$

$$J_b = 2,7 \cdot 10^{-6} Kgm^2$$

$$i = 0,056$$

$$T_{f,b} \approx T_{f,m} \approx 6 \cdot 10^{-6} Nm$$

$$\Rightarrow F_{disturb} = 0,19N$$

Required:

$$F_{cont} = 2N$$

$$F_{peak} = 5N$$

Obtained with this motor:

$$F_{cont} = 3,5N$$

$$F_{peak} = 7N$$

The button force and maximum friction meet the requirements, with the assumed maximum pressing movement.

The button force only occurs in one direction: the surgeon pushes it inwards, and the motor generates a force on the button outwards. When the surgeon releases the button, the gripper instrument in the eye returns to its neutral position. Therefore, also the button must return to its neutral, outer position. This is done by a tension spring (6). The spring force is able to overcome friction forces of the button and motor bearings as well as the gear friction and gravitational force on the button.

4.4.2 Backlash

Because the force feedback is in one direction, backlash of the meshing gears can be eliminated by the motor by always putting a small positive torque on it. Then, the pinion teeth will always mesh with the button gear and there is no backlash. This positive torque can also eliminate the need for a spring as discussed above. The button will always return in its outer position.

4.4.3 Resolution

On the motor shaft, an encoder disk (7) is mounted. The encoder house (8) can generate 400 *cpt*. With (4.10):

$$l = r_b$$

$$\Rightarrow R_b = 2 \cdot 10^{-5} m$$

This is less than the maximum required resolution of $R \leq 5 \cdot 10^{-5} m$, therefore this encoder meets the requirement.

4.4.3 Cable

To connect the motor and encoder with the θ -z block, a flat cable (9) is used. The θ rotation and z translation must be overcome. The flat cable is wound up in a similar way the flat cable in φ and ψ is, but a z stroke is added (figure 4.17).

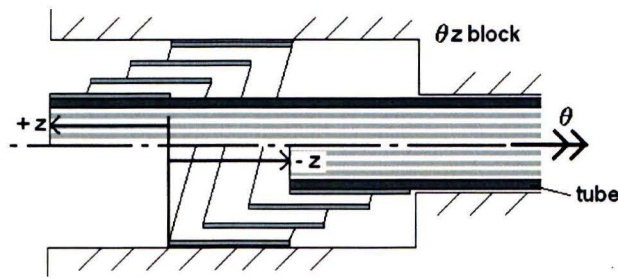


Figure 4.17: θ and z cable winding

Without high disturbance forces (discussed in paragraph 4.3.5), the cables are connected to the θ - z block. At the bottom of the pen, adding space to coil the cable would lead to larger distance between the button and the first rotation/translation bearing, which lowers the stiffness at the actuated position (discussed in 4.3.3.5). Therefore, the cable is transported to the top of the pen to coil it there. A tube (10) guides the cable through the cylinder ((2) in figure 4.7 on p.20). It is attached to the button part by a connector (11) in figure 4.16 on p.31 and thereby it rotates and translates along. To align the tube to the button part, the button part has a tube guide (12) with sliding fit for the tube.

4.4.4 Button fastening

The whole button part can easily be mounted on the pen by a coupling nut (13) which joins the button coupling bush (14) to the button housing (15). The pen can be modified for different surgeries by putting different button parts on. Then, the cable can be disconnected by the connector. Different functions can later be assigned to different buttons within the limits of the flexible cable.

4.5 Weight compensation

The gravitational force (F_g) acting from the centre of mass of the pen causes a force on the hand of the surgeon (F_{hand}), depending on the position the pen is in. In every degree of freedom (φ , ψ , θ and z) different parts, and thereby masses, add up to this disturbance force.

4.5.1 φ and ψ compensation

In the ψ -rotation only the θ -z part rotates and therefore the unbalance of this rotating mass causes a disturbance force in ψ direction. In the φ -rotation the θ -z part and the ψ part rotate together, and the unbalance of the sum of the centers of mass of these parts causes a disturbance force in φ rotation. In figure 4.18 the position of the centers of mass in φ and ψ rotation is shown. The z stroke slightly influences these positions. For mass compensation z is taken in its mid position.

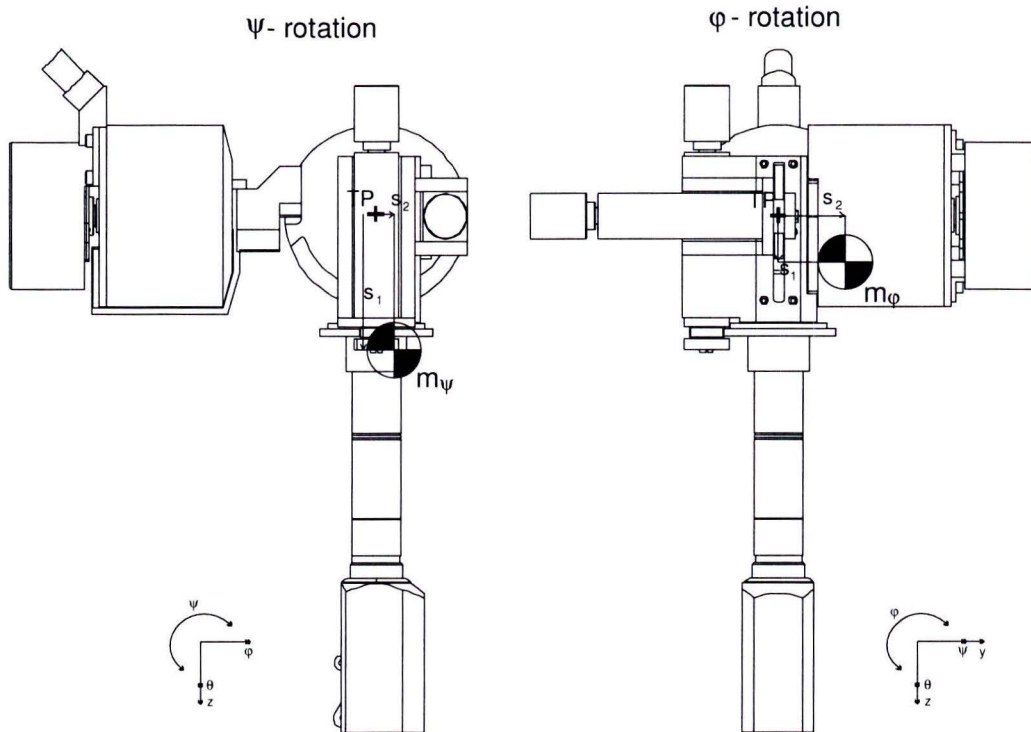


Figure 4.18: Centers of mass in φ and ψ rotation

In figure 4.19 a simplified version of the pen during one of these rotations is shown.

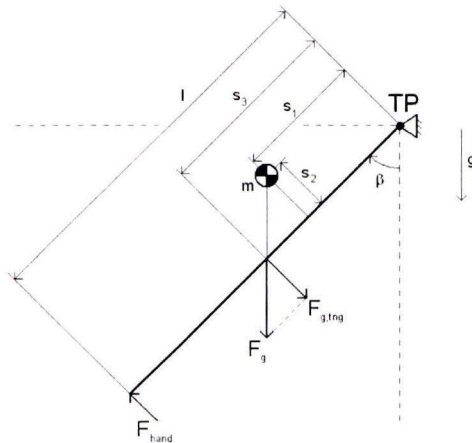


Figure 4.19: disturbance force caused by unbalance

The hand, at distance l , must apply a force to compensate for the tangential component ($F_{g,tng}$) of the gravitational force acting on the mass m . F_{hand} can be calculated by the equilibrium of moments about virtual trocar point TP :

$$F_{hand} \times l + F_{g,tng} \times s_3 = 0 \quad (4.32)$$

With simple goniometry it can be seen that:

$$F_{g,tng} = F_g \cdot \sin(\alpha) \quad (4.33)$$

$$s_3 = s_1 + \frac{s_2}{\tan(\alpha)} \quad (4.34)$$

In the ψ rotation the angle β is given by:

$$\beta = \psi + 45^\circ$$

The maximum hand force occurs at $\psi = +42^\circ$, the maximum force on the hand can be calculated:

$$l = 1,5 \cdot 10^{-1} m$$

$$m_\psi = 5,9 \cdot 10^{-1} kg$$

$$F_g = 5,8 N$$

$$s_1 = 5,7 \cdot 10^{-2} m$$

$$s_2 = 3 \cdot 10^{-3} m$$

$$\beta = 87^\circ$$

$$\Rightarrow F_{hand} = 1,9 N$$

In the φ rotation the angle $\beta = \varphi$. The maximum hand force occurs at $\varphi = 24^\circ$ and is calculated with:

$$\begin{aligned}
 l &= 1,5 \cdot 10^{-1} m \\
 m_\psi &= 2 kg \\
 F_g &= 20 N \\
 s_1 &= 1,1 \cdot 10^{-2} m \\
 s_2 &= 2,5 \cdot 10^{-2} m \\
 \beta &= 24^\circ \\
 \Rightarrow F_{hand} &= 3,6 N
 \end{aligned}$$

This disturbance force is 60% respectively 140% of the required continuous force for the actuator in ψ and φ direction. The actuator can not be used to compensate for it, because all the torque it can deliver is needed for the force feedback.

To compensate for the unbalance a counter mass is used. First the ψ rotation is balanced. The center of mass of m_ψ and counter mass $m_{c,\psi}$ summed up, should coincide with the virtual trocar point TP. Then, the ψ rotation is balanced: the pen can be placed in any position without causing a reaction force on the surgeons' hand. To do so, a mass is placed above the pivoting point TP, where the centre of mass of the pen, the pivoting point and the centre of mass of the counter weight form a straight line in this 2D view (figure 4.20).

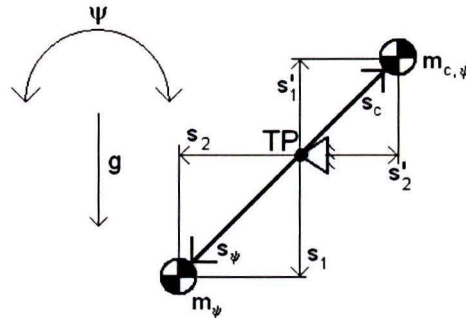


Figure 4.20: ψ counter mass placement

Also, the following must hold:

$$m_\psi \times s_\psi = m_{c,\psi} \times s_c \quad (4.35)$$

For compactness and to obtain the lowest inertia, a larger counter mass at smaller distance is favourable, where inertia is related to the mass and distance to pivoting point by:

$$inertia \propto m_c \times s_c^2 \quad (4.36)$$

A material with high density, Tungsten Carbide, is chosen. The density is $\rho = 1,7 \cdot 10^4 kg / m^3$ and this material is in stock.

This ψ counter mass is shifted in y (see figure 4.18 on p.35) to put its centre of mass in line with m_φ and TP. An additional mass is added for cancelling the small unbalance left, as tungsten carbide is difficult to machine. This mass is mounted axis symmetric in ψ to keep the ψ centre of mass unchanged. In figure 4.2, p.13, the resulting design is shown (in brown).

4.5.2 θ -compensation

Mass compensation in θ is not necessary, because all the bodies moving in θ are axis symmetric.

4.5.3 Z-compensation

The disturbance force caused by the z movement is only dependent on the pen position in φ and ψ . The maximum disturbance force in z direction is felt at the pen position $\varphi = 0^\circ$ and $\psi = -45^\circ$. In this position the pen is aligned with the gravitational vector. Then, $F = m \cdot g = 1,5N$. The disturbance force decreases proportional to the angle between pen and gravitational vector. For compensating in z , two concepts are made, the rack-pinion and pulley-string concept (figure 4.21).

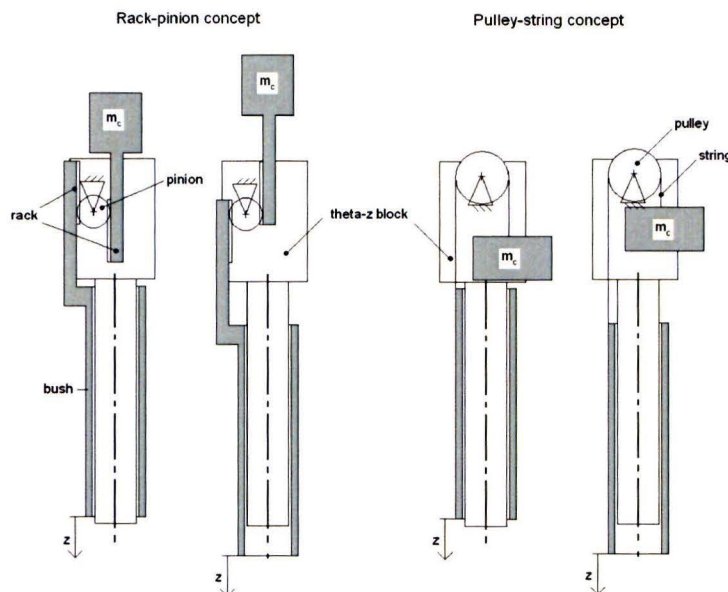


Figure 4.21: z mass compensation concepts

The upper and lower position of the bush is shown for both concepts. At the rack-pinion concept, two racks mesh with a pinion which is attached to the θ - z block. Moving the bush in z , both racks move the same distance in opposite direction. One rack is attached to a counter mass m_c with the same mass as the bush. Thereby, the z movement has been mass compensated for.

At the pulley-string concept the bush mass and counter mass are connected by a string. The direction alternation is done by a pulley, attached to the θ - z block. Both counter masses should be guided to allow only a z movement. The latter concept only works, when gravitation causes tension in the string ($-90^\circ < \varphi < +90^\circ$ and $\psi < +45^\circ$).

Both concepts introduce extra friction. In the present pen design, no space is available for this compensation. Mass compensation in the z movement has not been added. Testing the design must show the necessity for it.

As mentioned before, the z movement also introduces a disturbance force in the φ and ψ direction because in the z stroke the centers of mass shown in figure 4.18 on p.35 shift. The maximum hand force at $z = \pm 7,5$ mm in φ and ψ , without φ and ψ compensation, can be calculated by (4.32):

In ψ the only difference is:

$$\begin{aligned}l &= 1,5 \cdot 10^{-1} \pm 7,5 \cdot 10^{-3} \text{ m} \\s_1 &= 5,7 \cdot 10^{-2} \pm 2,5 \cdot 10^{-3} \text{ m} \\F_{hand,\psi} &= 1,9 \pm 0,1 \text{ N}\end{aligned}$$

In φ the only difference is:

$$\begin{aligned}l &= 1,5 \cdot 10^{-1} \pm 7,5 \cdot 10^{-3} \text{ m} \\s_1 &= 1,1 \cdot 10^{-2} \pm 1,5 \cdot 10^{-3} \text{ m} \\F_{hand,\varphi} &= 3,6 \pm 0,1 \text{ N}\end{aligned}$$

These forces are below the requirement of for the friction force in φ and ψ and therefore, no extra measurements are taken to cancel out these disturbance forces. Also, this force is proportional to the z stroke and therefore feed forward can be used to cancel it.

4.6 Performance

In table 4.1 a summary is given of the required and obtained feedback force and torque, friction force and torque and resolution (requirements from table 3.1).

Table 4.1: Performance of the designed haptic pen

DOF	Variable	Requirement	Obtained
φ	F_{cont}	$\geq 2,5N$	$3N$
	F_{peak}	$\geq 10N$	$11N$
	F_f	$\leq 0,2N$	$< 0,3N$
	R	$\leq 5 \cdot 10^{-5} m$	$30 \cdot 10^{-6} m$
	<i>Range</i>	$\pm 45^\circ$	$\pm 90^\circ$
ψ	F_{cont}	$\geq 2,5N$	$3N$
	F_{peak}	$\geq 10N$	$11N$
	F_f	$\leq 0,2N$	$< 0,3N$
	R	$\leq 5 \cdot 10^{-5} m$	$30 \cdot 10^{-6} m$
	<i>Range</i>	$\pm 45^\circ$	$+45^\circ$ to -88°
θ	F_{cont}	$\geq 30 \cdot 10^{-3} Nm$	$49 \cdot 10^{-3} Nm$
	F_{peak}	$\geq 50 \cdot 10^{-3} Nm$	$6,5 \cdot 10^{-1} Nm$
	F_f	$\leq 2 \cdot 10^{-3} Nm$	$3 \cdot 10^{-3} Nm$
	R	$\leq 5 \cdot 10^{-5} m$	$11 \cdot 10^{-6} m$
	<i>Range</i>	$\pm 90^\circ$	$\pm 175^\circ$
z	F_{cont}	$\geq 2,5N$	$2,4N$
	F_{peak}	$\geq 5N$	$32N$
	F_f	$\leq 0,2N$	$< 0,3N$
	R	$\leq 5 \cdot 10^{-5} m$	$\leq 1,8 \cdot 10^{-6} m$
	<i>Range</i>	$\pm 7,5 \cdot 10^{-3} m$	$\pm 8 \cdot 10^{-3} m$
button	F_{cont}	$\geq 2N$	$3,5N$
	F_{peak}	$\geq 5N$	$7N$
	F_f	$\leq 0,2N$	$< 0,2N$
	R	$\leq 5 \cdot 10^{-5} m$	$20 \cdot 10^{-6} m$
	<i>Range</i>	$5 \cdot 10^{-3} m$	$5 \cdot 10^{-3} m$

As can be seen from the table all feedback forces except the F_{cont} in z direction meet the requirements. This force is slightly smaller. Because the requirements are based on coarse approximations, this small difference will not influence the total performance of the haptic pen.

The friction torque and force in φ-, ψ-, θ-, and z is 50% larger than the requirement. The requirement is based on a noticeable force deviation of 7% of the applied force (paragraph 3.3). Therefore, the obtained friction will be felt by the surgeon. However, in θ and z 33% of the friction force and torque is caused by the cable, which is proportional to the θ and z movement.

With feed forward this can be canceled out. In φ and ψ 33% of the friction force is generated by the gravitational force on the shifting pen in z . It is proportional to the z stroke and therefore again with feed forward this can be canceled out. Then, all the friction levels will meet the requirements.

All the ranges meet the requirements.

All the resolutions of the encoders meet the requirements. However, to be able to measure the real pen tip movement with this resolution, the stiffness should exceed $c \geq 2,1 \cdot 10^5 \text{ N/m}$ according to (3.2) and (3.3) on p.9. In appendix C the stiffness of all parts in φ , ψ , θ and z direction is calculated. For each DOF the total stiffness can be determined by:

$$\frac{1}{c_s} = \frac{1}{c_1} + \dots + \frac{1}{c_n} \quad (4.37)$$

where c_1 to c_n are the separate stiffness's of the individual parts and contacts, serially linked. The lowest stiffness in each direction is the limiting stiffness, stated in table 4.2. The torsional stiffness in θ is converted to a translational stiffness at the radius $r = 1 \cdot 10^{-2} \text{ m}$ where the surgeon holds the pen, by:

$$c_\theta = \frac{k_\theta}{r^2} \quad (4.38)$$

Table 4.2: limiting stiffness in φ , ψ , θ and z

DOF	Limiting part	Stiffness [N/m]
φ	φ -bearings	$6 \cdot 10^5$
ψ	φ -house	$5 \cdot 10^5$
θ	motor shaft	$8 \cdot 10^6$
z	ψ -house	$3 \cdot 10^5$

The stiffness meets the requirements. The maximum deflection is $8 \cdot 10^{-6} \text{ m}$ and maximum virtual backlash is $1 \cdot 10^{-6} \text{ m}$. Adding the latter to the resolution obtained by the encoders, the total resolution meets the requirement of $R \leq 5 \cdot 10^{-5} \text{ m}$ in all DOF.

This resolution is based on a static loading. A human being is able to move his hand with a frequency of approximately 20 Hz (the surgeon probably uses lower hand frequencies during eye-surgery). The first eigen-frequency of the pen should be higher than this value, to be able to measure the real hand movements with the encoders. Using a 1-dimensional mass-spring analysis an approximation is made for the lowest eigen-frequency, given by:

$$\omega_n = 2\pi \sqrt{\frac{c}{m}} \quad (4.39)$$

For the mass a worst case value is taken of 2 kg. With the lowest stiffness from table 4.2 the eigen-frequency is:

$$\Rightarrow \omega_n = 60 \text{ Hz}$$

This is factor 3 higher than the maximum hand frequency and therefore, the stiffness is sufficient.

5 Conclusions and recommendations

A design for a 5 DOF haptic master device for an eye-surgery robot has been made and the prototype is built. The design meets the feedback force and torque and range requirements as determined before the project started. Testing of the haptic pen must show if these requirements come up to expectations.

A first analysis has been made with respect to the friction force felt by the surgeon. This indicates that the friction force and friction torque is not noticeable by the surgeon. Thereby, it meets the requirements. Measurements of the friction of all components must confirm if this is the case.

The resolution of the encoders is at least factor 1,7 higher than the requirements. The static and dynamic loading influence the actual measurable hand movement, thereby lowering the resolution. A first analysis of static and dynamic behaviour indicates that the resolution meets the requirements. Testing of the haptic pen must show if the resolution is high enough to truly provide a haptic feeling to the surgeon's hand.

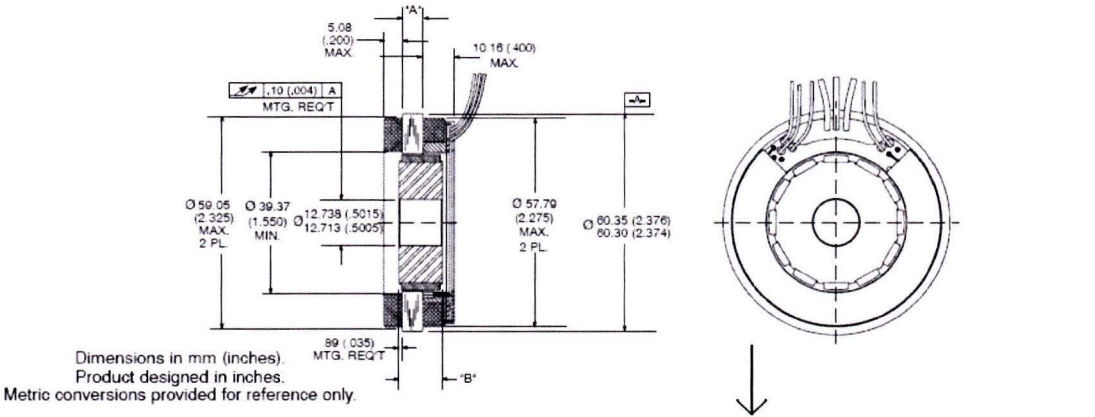
Bibliography

- [1] Vanja Bozovic. Medical Robotics, I-Tech Education and Publishing, Vienna Austria, 2008.
- [2] Jessie Y.C. Chen, Ellen C. Haas and Michael J. Barnes. Human Performance Issues and User Interface Design for Teleoperated Robots, IEEE Transactions on Systems, Man and Cybernetics-Part C: Applications and reviews, vol. 37, No. 6, November 2007.
- [3] C. N. Riviere, R.S. Rader, and P. Khosla. Characteristics of hand motion of eye surgeons, 19th Annual Conference of the IEEE Engineering in Medicine and Biology Society, Chicago, October, 1997, pp. 1690 – 1693.
- [4] X.D. Pang, H.Z. Tan, and I. Durlach. Manual discrimination of force using active finger motion. *Perception & Psychophysics*, 49(6):531-540, 1991.
- [5] P.C.J.N. Rosielle and E.A.G Reker. Constructieprincipes 1 – bedoeld voor het nauwkeurig positioneren, Lecture note 4007, 2004.
- [6] Roloff / Matek. Maschinenelemente; Normung, Berechnung, Gestaltung, 13. Auflage. Friedr. Vieweg & Sohn Verlagsgesellschaft mbH, Braunschweig/Wiesbaden, 1994.
- [7] Informatieblad radiale- of axiale stijfheid van kogellagers en kogelparen, Philips CFT.
- [8] SKF. Hoofdcatalogus wentellagers, 1976.
- [9] Dubbel. Taschenbuch für den Maschinenbau, 16. Auflage. Springer-Verlag Berlin Heidelberg New York London Paris Tokyo, 1987.
- [10] Eriks. Technical Documentation o-rings
- [11] Fujikura. Flat Flexible Cables, <http://www.fujikura.co.uk>, 2008.
- [12] C.J. Snijder, Toepassing en berekening van metalen veren voor kleine werktuigen, Lecture note 415, 1968.
- [13] Reliance, Instrumentation Gears, 2007.
- [14] Systematic BV, lineaire en roterende geleidingen, <http://www.systematic.nl>, 2008

A Datasheets purchased parts

A1 ϕ and ψ brushless Kollmorgen motor

RBE-0151X-X00



Dimensions in mm (inches).
Product designed in inches.
Metric conversions provided for reference only.

- Notes:
- 1) For a C.W. rotation, as viewed from lead end, energize per excitation sequence table.
 - 2) V-AB, V-BC and V-CA is back EMF of motor phases AB, BC and CA respectively, aligned with sensor output as shown for C.W. rotation only.
 - 3) Mounting surface is between ϕ 60.35 (2.376) and ϕ 59.06 (2.325) on both sides.

MODEL NUMBER	RBE-01510	RBE-01511	RBE-01512	RBE-01513	RBE-01514	RBE-01515	RBE-01516
"A" Dimension	5.72 (0.225)	12.7 (0.500)	19.05 (0.750)	25.4 (1.000)	33.02 (1.300)	38.1 (1.500)	50.8 (2.000)
"B" Dimension	12.07 (0.475)	19.05 (0.750)	25.4 (1.000)	31.75 (1.250)	39.37 (1.550)	44.45 (1.750)	57.15 (2.250)
Tolerance \pm .010 on "A" Dimension.							

RBE(H) Motor Series

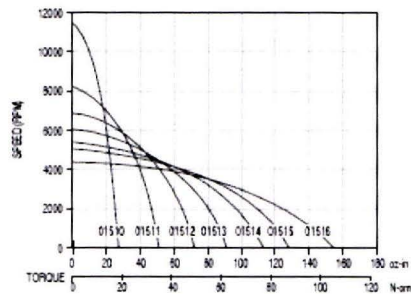
RBE(H) 01510 MOTOR SERIES PERFORMANCE DATA

Motor Parameters	Symbols	Units	01510	01511	01512	01513	01514	01515	01516	
Max Cont. Output Power at 25°C amb.	HP Rated	HP	0.127	0.176	0.210	0.240	0.264	0.284	0.307	
	P Rated	Watts	95	131	157	179	197	212	229	
Speed at Rated Power	N Rated	RPM	7450	5400	4550	4050	3570	3400	2970	
Max Mechanical Speed	N Max	RPM	16500	16500	16500	16500	16500	16500	16500	
Continuous Stall Torque at 25°C amb.	Tc	oz-in	27.4	54.3	71.9	91.3	114	127	154	
		N-m	0.193	0.384	0.508	0.645	0.808	0.897	1.085	
Peak Torque	Tp	oz-in	78.6	162	234	313	403	540	610	
		N-m	0.555	1.15	1.66	2.21	2.85	3.81	4.31	
Max Torque for Linear KT	Tsl	oz-in	78.6	162	234	313	403	540	610	
		N-m	0.555	1.16	1.66	2.21	2.85	3.81	4.31	
Motor Constant	Km	oz-in/√W	6.38	11.6	14.8	18.2	22.1	24.1	28.6	
		N-m/√W	0.0451	0.0819	0.105	0.128	0.156	0.170	0.202	
Thermal Resistance*	Rth	°C/Watt	4.10	3.55	3.30	3.13	2.95	2.85	2.72	
Viscous Damping	Fi	oz-in/RPM	2.74E-04	1.05E-03	1.76E-03	2.47E-03	3.32E-03	3.88E-03	5.30E-03	
		N-m/RPM	1.94E-06	7.43E-06	1.24E-05	1.74E-05	2.34E-05	2.74E-05	3.74E-05	
Max Static Friction	Tf	oz-in	2.00	2.93	3.77	4.62	5.63	6.31	8.00	
		N-m	0.0141	0.021	0.027	0.033	0.040	0.045	0.057	
Max Cogging Torque	Toog	oz-in	0.950	1.22	1.47	1.71	2.01	2.21	2.70	
		N-m	0.00671	0.00862	0.0104	0.0121	0.0142	0.0156	0.019	
Frameless Motor	Weight	Wrf	oz	6.30	10.5	14.3	18.1	22.7	25.8	33.4
			Kg	1.79E-01	2.98E-01	4.06E-01	5.14E-01	6.44E-01	7.30E-01	9.47E-01
Housed Motor	Weight	Wth	oz	19.0	23.5	27.5	31.6	36.4	39.7	47.8
			Kg	5.39E-01	6.65E-01	7.80E-01	8.95E-01	1.03E+00	1.13E+00	1.38E+00
No. of poles	P		12	12	12	12	12	12	12	

Winding Constants	Symbols	Units	A	B	C	A	B	C	A	B	C	A	B	C	A	B	C	A	B	C			
Current at Cont. Torque	Ic	Amps	5.10	3.71	9.06	4.85	3.53	4.98	4.44	3.23	7.90	4.22	3.07	7.50	4.62	2.94	7.18	5.13	2.83	6.91	5.18	2.59	6.34
Current at Peak Torque	Ip	Amps	14.0	9.89	25.0	14.0	9.89	16.7	14.0	9.89	25.0	14.0	9.89	25.0	15.7	9.89	25.0	21.0	9.89	25.0	19.8	9.89	25.0
Torque Sensitivity	Kt	oz-in/Amp	6.78	7.92	3.24	11.6	16.2	11.5	17.0	23.4	9.56	22.7	31.2	12.8	26.0	40.9	16.7	26.0	47.2	19.3	31.2	62.3	25.5
		N-m/Amp	0.0407	0.0559	0.0229	0.0833	0.115	0.0812	0.120	0.165	0.0675	0.160	0.220	0.0901	0.184	0.289	0.118	0.184	0.333	0.136	0.220	0.440	0.180
Back EMF constant	Eb	V/KRPM	4.26	5.86	2.40	8.73	12.0	8.50	12.6	17.3	7.07	16.8	23.1	9.43	19.2	30.2	12.4	19.2	34.9	14.3	23.1	46.1	18.9
Motor Resistance	Rm	Ohms	0.814	1.58	0.256	1.04	2.02	0.988	1.33	2.59	0.418	1.55	3.03	0.489	1.38	3.45	0.557	1.16	3.86	0.623	1.19	4.75	0.789
Motor Inductance	Lm	mH	0.32	0.81	0.101	0.58	1.1	0.55	0.87	1.6	0.27	1.2	2.3	0.38	1.1	2.6	0.47	0.99	3.3	0.55	1.1	4.4	7.4

*Rth assumes a housed motor mounted to a 4" x 3.25" x 0.25" aluminum heatsink or equivalent

Continuous Duty Capability for 130°C Rise — RBE - 01510 Series



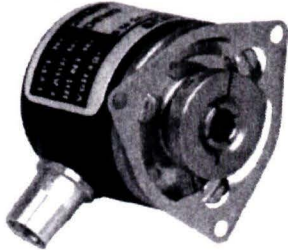
A2 ϕ and ψ Scancon encoder



SCANCON®

CE TYPE 2RMHF

24 mm diameter - up to 7500 pulses/turn
up to 30000 counts



Also as Absolute SSI - Section 14 page 1 to 2

CHARACTERISTICS

ENCODER TYPE	Hollow shaft encoder (blind end)
SMD - TECHNOLOGY	Strong compact electronics
HIGH IP-RATING	Std. IP 64 (option: Ribbon cable + DC connector = IP50)
LOW CURRENT CONSUMPTION	To be connected directly to PLC'S and counters
SHORT CIRCUIT PROTECTION	Thermal shut down at 155°C
WIDE SUPPLY RANGE	Min. 4.5V to max 30V
STRONG CONSTRUCTION	Based on 2 precision ball bearings, for industrial environments

ELECTRICAL SPECIFICATIONS

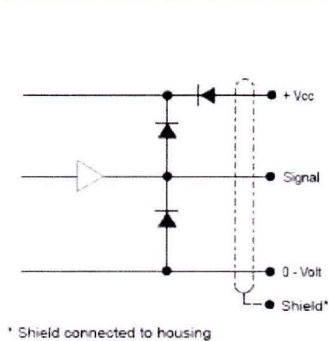
	At +25°C
Output	Totempole
Output waveform	Incremental (A, B)
Zero or index pulse	(Z) one pr./rev.
Supply-voltage (V _{in})	Min 4.5V to Max. 30V * Reverse polarity protection
Current (no load)	35mA
Max. load pr. output	20mA (Short circuit protected)*
V _{out} low	Max. 500 mV @ I = 10 mA
Operating temp.	-40°C to +85°C
Storage temp.	-40°C to +85°C
Max. pulse frequency	200 kHz *
V _{out} high	Min. (V _{in} - 0,8) @ I = -10mA Min. (V _{in} - 1,3) @ I = -25mA
Cable data	5(0,14 mm ²) or 8-leads(0,05mm ²) shielded
Output signals	Standard, Inverted Differential (RS-422A compatible)
Certified acc. to	EN 50081-1 and EN 50082-2

* = It is not recommended to combine max value for all 3 parameters

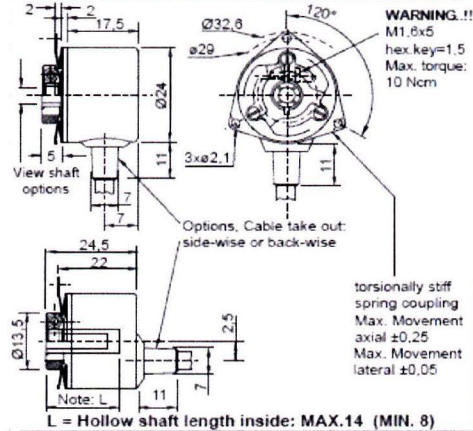
MECHANICAL SPECIFICATIONS

Weight	About 35 g (+cable = 0,040 Kg/meter)
Materials: Housing	Electroplated steel and brass
Shaft	Brass
Bearings	Lifetime lubricated ball-bearings
Fix. clamp	Brass
H.-Shaft dimensions	View Ordering Code, next page
H.-Shaft loads	Axial max. 20 N Radial max. 20 N
Max. rev.	12.000 rev./min
IP-rating	IP 64
Start torque	<0,005 Nm at 25°C
Mass moment of inertia	1,0 gcm ²
Max. shock	100 G/11 ms.
Bump	10 G - 16 ms (1000 x 3 axis)
Vibration	(10 - 2000 Hz) 1/10 G

OUTPUT CIRCUIT



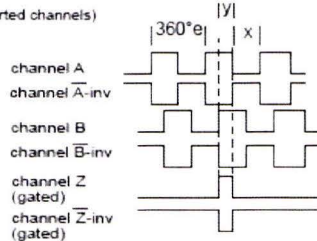
MECHANICAL DIMENSIONS



OUTPUT WAVEFORM

Rotation: Clockwise (cw) from shaftside

(inv = inverted channels)



$X = 180^\circ e \pm 36^\circ e$ and $Y = 90^\circ e \pm 18^\circ e$
Z-puls: Gated with A and B (standard)

Options: TTL or HTL compatible. Open Collector NPN or PNP
Gated Z-puls or none-gated Z-puls.
View more Output options in section 16 - page 1 to 2

CONNECTIONS

Color code	Standard	Color code	Differential
Green	Ch A	Pink	Ch A
Yellow	Ch B	Grey	Ch A inv
Grey	Ch Z	Green	Ch B
Brown	Vcc	Yellow	Ch B inv
White	0-Volt	White	Ch Z
		Brown	Ch Z inv
		Red	Vcc
		Blue	0-Volt

PULSES/REV.

4	30	100	250	600	2048
10	36	125	256	1000	2500
11	50	128	300	1024	3000
12	60	150	360	1250	3600
15	75	180	400	2000	5000
25	90	200	500	2500	7500

ORDERING CODES

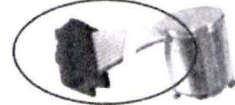
	Options	Order code
Pulses pr.rev.:	No. of pulses	XXXX
Output signal:	Normal (TP-Standard) 3 channel = A, B, Z	N
	TP-Differential, 6 channel A, B, Z and A-inv, B-inv, Z-inv	D
Hollow Shaft Dimensions: (Tolerance G7)	ø3 mm ø4 mm ø5 mm ø8 mm ø1/4"	03 04 05 08 1/4
IP-rating:	IP 64	64
Round Cable Length of cable:	Standard 1 meter No. of meters	01 XX
Round Cable take out:	Side Back	S B
Cable and connector options:	View section 15 page 10 to 14	
Anti rotation spring coupling or Flange / Plate:	View Section 8 page 9 to 13	

Flat Ribbon Cable and/or Connector

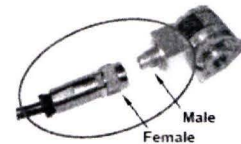
View section 15 page 10 to 14

Options

Flat Cable (only IP 50)
Ribbon + IDC or AMP



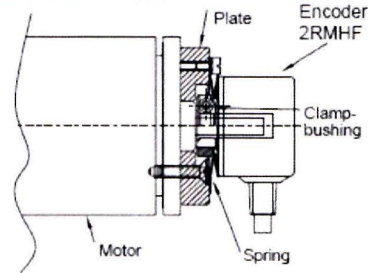
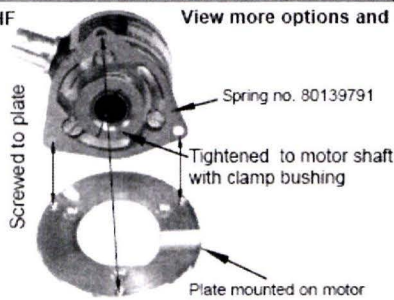
Connector on Encoder:
(only IP64)



CHARACTERISTICS: For montage on motor or other unit.

2RMHF

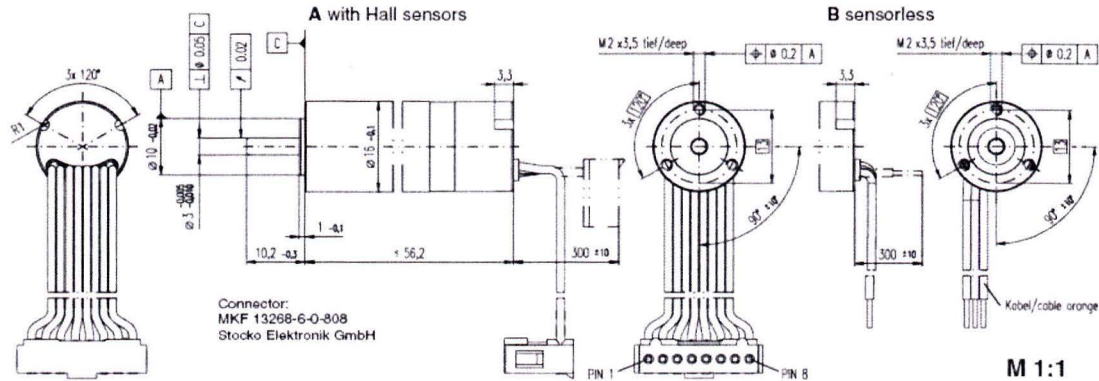
View more options and accessories in Section 9 page 1 to 6



2RMHF **7500** **D** **06** **50** **01** **S** **80139791** **IDC**
Pulses Output signal Hollow Shaft IP-rating Length of round cable Cable take out Anti Rotation Spring Coupling cable connector

A3 θ and z brushless Maxon motor

EC 16 Ø16 mm, brushless, 40 Watt



- Stock program
- Standard program
- Special program (on request)

	Order Number			
A with Hall sensors	232242	262960	232241	262662
B sensorless	235990	262664	236696	262866

Motor Data					
Values at nominal voltage					
1 Nominal voltage	V	12.0	18.0	24.0	32.0
2 No load speed	rpm	35900	40300	41400	41400
3 No load current	mA	358	284	222	166
4 Nominal speed	rpm	32100	36700	37900	37900
5 Nominal torque (max. continuous torque)	mNm	13.3	13.4	13.9	13.8
6 Nominal current (max. continuous current)	A	4.51	3.41	2.71	2.03
7 Stall torque	mNm	141	166	184	183
8 Starting current	A	44.5	39.3	33.5	24.9
9 Max. efficiency	%	83	84	85	85
Characteristics					
10 Terminal resistance phase to phase	Ω	0.269	0.458	0.716	1.28
11 Terminal inductance phase to phase	mH	0.0140	0.0249	0.0420	0.0746
12 Torque constant	mNm / A	3.18	4.23	5.50	7.33
13 Speed constant	rpm / V	3010	2260	1740	1300
14 Speed / torque gradient	rpm / mNm	255	244	226	228
15 Mechanical time constant	ms	3.39	3.25	3.01	3.03
16 Rotor inertia	gm ²	1.27	1.27	1.27	1.27

Specifications	Operating Range	Comments
Thermal data 17 Thermal resistance housing-ambient 10.3 K / W 18 Thermal resistance winding-housing 1.2 K / W 19 Thermal time constant winding 2.08 s 20 Thermal time constant motor 299 s 21 Ambient temperature -20 ... +100°C 22 Max. permissible winding temperature +125°C Mechanical data (preloaded ball bearings) 23 Max. permissible speed 50000 rpm 24 Axial play at axial load < 3.5 N 0 mm > 3.5 N max. 0.14 mm 25 Radial play preloaded 26 Max. axial load (dynamic) 3 N 27 Max. force for press fits (static) (static, shaft supported) 40 N 250 N 28 Max. radial loading, 5 mm from flange 10 N		<p>Continuous operation In observation of above listed thermal resistance (lines 17 and 18) the maximum permissible winding temperature will be reached during continuous operation at 25°C ambient. = Thermal limit.</p> <p>Short term operation The motor may be briefly overloaded (recurring).</p> <p>— Assigned power rating</p>
Other specifications 29 Number of pole pairs 1 30 Number of phases 3 31 Weight of motor 58 g	maxon Modular System Planetary Gearhead Ø22 mm 0.5 - 2.0 Nm Page 232	Overview on page 16 - 21 for type A: Encoder MR 128 / 256 / 512 CPT, Page 257

Values listed in the table are nominal.

Connection A

brown	Motor winding 1	Pin 1
red	Motor winding 2	Pin 2
orange	Motor winding 3	Pin 3
yellow	V _{Hall} 4.5 ... 24 VDC	Pin 4
green	GND	Pin 5
blue	Hall sensor 1	Pin 6
violet	Hall sensor 2	Pin 7
grey	Hall sensor 3	Pin 8

Connection B (Cable AWG 24)

brown	Motor winding 1
red	Motor winding 2
orange	Motor winding 3

Wiring diagram for Hall sensors see page 27

- Recommended Electronics:**
- | | |
|--------------------|----------|
| DECS 50/5 | Page 284 |
| DEC 24/3, DEC 50/5 | 285 |
| DECV 50/5 | 286 |
| DIES 50/5 | 287 |
| EPOS 24/1 | 294 |
| EPOS 24/5 | 294 |
| EPOS2 50/5 | 295 |
| EPOS P 24/5 | 297 |
| Notes | 20 |

A4 θ and z Scancon encoder

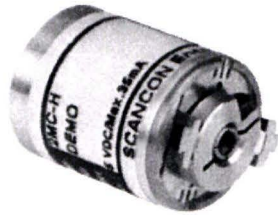


SCANCON®



TYPE 2MCH

Only 16mm in diameter and up to 5000 ppr. -True lines.
Up to 20000 Counts



CHARACTERISTICS

ENCODER TYPE	Micro hollow shaft encoder (blind end hollow shaft)
SMD - TECHNOLOGY	Strong compact electronics
HIGH IP-RATING	Std. IP 64 (with IDC; IP 50)
LOW CURRENT CONSUMPTION	To be connected directly to PLC'S and counters
SHORT CIRCUIT PROTECTION	Thermal shut down at 155°C
POWER SUPPLY	5 volts to 12 Volts \pm 10% (TTL) (on request up to 24 Volts)
STRONG MEC. CONSTRUCTION	Based on 2 precision ball bearings for industrial environment

ELECTRICAL SPECIFICATIONS

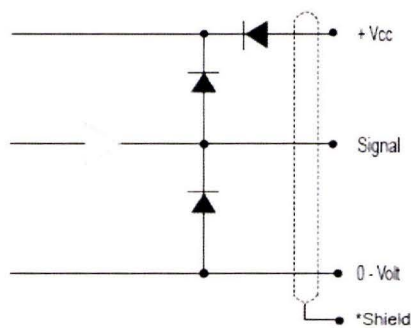
At +25°C	
Output	Totempole
Output waveform	Incremental (A, B)
Zero or index pulse	(Z) one pr./rev.
Supply-voltage	5 to 12 V (on request up to 24 Volts)
Current (no load)	35mA
Max. load pr. output	20mA (Short circuit protected)
V out low	Max. 500 mV at I out low = 10 mA
Operating temp.	-20°C to +70° C
Storage temp.	-20° C to +85°C
Max. pulse frequency	200 kHz
V out high	Min. (Vin -0.8) @ I = -10mA Min. (Vin -1.3) @ I = -25mA
Cable data	8-leads (0.05 mm ²) shielded or 10-leads flat band cable 0.10mm ²
Output signals	Differential (RS-422A compatible)
Certified acc. To	EN 50081-1 and EN 50082-2*

*NA with flat band cable

MECHANICAL SPECIFICATIONS

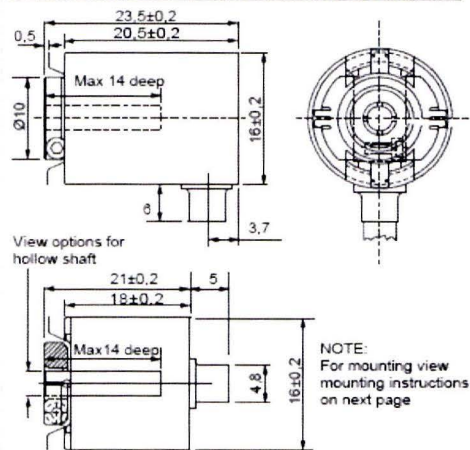
Weight, excl. Cable	About 15 g
Materials:	
Housing	Brass / Aluminum
Shaft	Brass
Bearings	Lifetime lubricated ball-bearings
Fixing clamp	Brass
H.-Shaft dimensions	ϕ 1.5mm - ϕ 2mm - ϕ 3mm - 1/8"
H.-Shaft loads	Axial max. 10 N Radial max. 10 N
Max speed	12,000 rev./min.
IP-rating	IP 64 (with IDC; IP 50)
Start torque	<0,005 Nm at 25°C
Massmoment of inertia	0.25 gm ²
Max. shock	100 G/11 ms
Bump	10 G - 16 ms (1000 x 3axis)
Vibration	(10 - 2000 Hz) 10 G

OUTPUT CIRCUIT




*Shield connected to housing

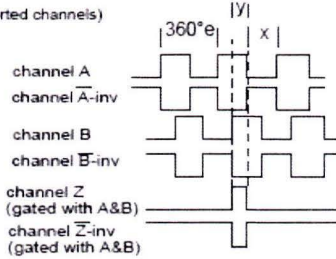
MECHANICAL DIMENSIONS



OUTPUT WAVEFORM

 Rotation: Clockwise (cw) from shaftside

(inv = inverted channels)



$X = 180^\circ e \pm 36^\circ e$ and $Y = 90^\circ e \pm 18^\circ e$
Z puls: Gated with A and B (standard)

Options: Open Collector NPN or PNP
Gated Z-puls or none-gated Z-puls.
View more Output options in section 15 - page 1

ORDERING CODES

	Options	Order code
Pulses pr. Rev.:	No. of pulses	XXXX
Output signal:	TP-Differential, 8 channel A, B, Z and A-inv, B-inv, Z-inv	D
H.-Shaft dimensions:	$\phi 1,5\text{mm}$ $\phi 2,0\text{mm}$ $\phi 3,0\text{mm}$ 1/8"	1,5 2,0 3,0 1/8
IP-rating:	IP 64 Standard	64
Length of cable:	Standard 1 meter No. of meters	01 XX
Cable take out:	Side Back	S B
Anti rotation spring coupling Or Flange / Plate:	View Section 9 page 1 to 8	
Flat Ribbon Cable + IDC:	View Section 20 page 10	

CONNECTIONS

8 leads cable

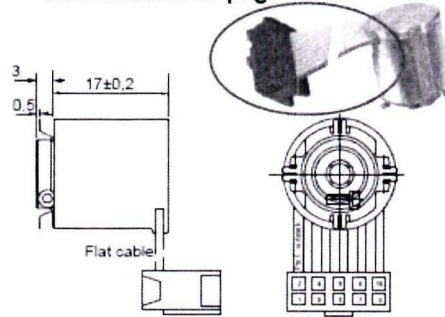
Color code	Differential
Pink	Ch A
Grey	Ch A inv
Green	Ch B
Yellow	Ch B inv
White	Ch Z
Brown	Ch Z inv
Red	Vcc
Blue	0-Volt

PULSES/REV.

100	300	500	2000	3600
125	360	1024	2500	5000

Flat Ribbon Cable and/or Connector

View Section 20 page 10

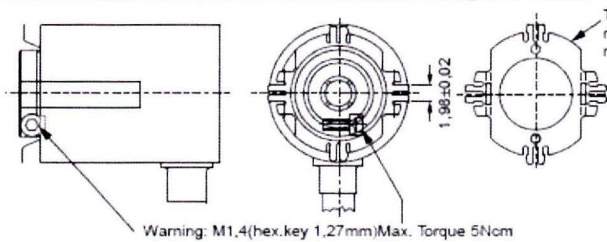


Advanced Output Options:

Options	Ordering codes
Normal Open Collector NPN	NON
Differential Open Collector NPN	DON
Normal Open Collector PNP	NOP
Differential Open collector PNP	DOP

To order replace with
Output signal

Mounting instructions



Torsionally stiff spring coupling
max. movement axial = $\pm 0,1$
max. movement radial = $\pm 0,05$

When using motors with axial play, encoder should be mounted with motor shaft pushed as far as possible into the hollow shaft, while supplying the back cover of the encoder with slight pressure, when tightening the fixing clamp.

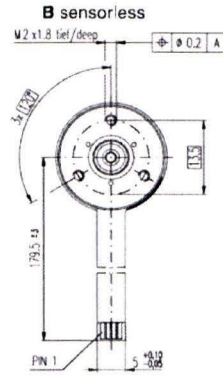
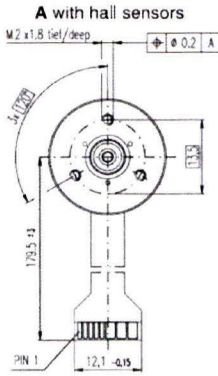
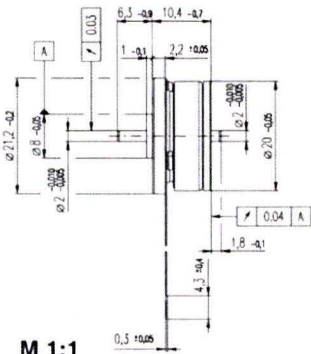
Remark:
Short circuit protection / reverse polarity protection

2MCH
Pulses Output signal Shaft IP-rating Length of round cable Cable take out Anti Rotation Spring Coupling Or Flange / Plate Order Number

A4 button brushless Maxon motor

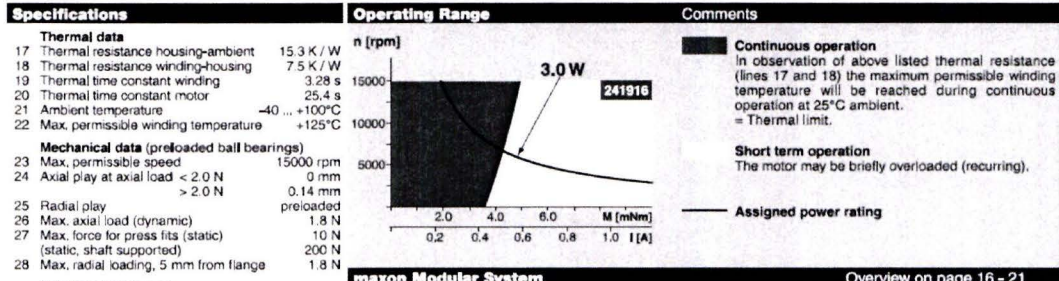
maxon flat motor

EC 20 flat Ø20 mm, brushless, 3 Watt



Order Number	351098	241916	351100	351101
A with hall sensors	351098		351100	351101
B sensorless	339255	241916	330257	330258

Motor Data		Values at nominal voltage				
1	Nominal voltage	V	6.0	9.0	12.0	24.0
2	No load speed	rpm	8960	9630	9370	9310
3	No load current	mA	62.5	44.9	33.1	16.2
4	Nominal speed	rpm	3160	4230	3530	3840
5	Nominal torque (max. continuous torque)	mNm	3.07	3.91	3.16	3.67
6	Nominal current (max. continuous current)	A	0.548	0.470	0.292	0.163
7	Stall torque	mNm	5.29	8.04	5.67	7.12
8	Starting current	A	0.900	0.957	0.503	0.309
9	Max. efficiency	%	55	62	56	60
Characteristics						
10	Terminal resistance phase to phase	Ω	6.67	9.40	23.9	77.7
11	Terminal inductance phase to phase	mH	0.639	1.30	2.35	9.80
12	Torque constant	mNm / A	5.88	8.40	11.3	23
13	Speed constant	rpm / V	1620	1140	847	414
14	Speed / torque gradient	rpm / mNm	1840	1270	1790	1400
15	Mechanical time constant	ms	74.1	51.2	72.1	56.2
16	Rotor inertia	gcm ²	3.84	3.84	3.84	3.84



Other specifications		maxon Modular System		Overview on page 16 - 21	
29	Number of pole pairs	4	Spur Gearhead	Ø20.3 mm	Page 227
30	Number of phases	3	Planetary Gearhead	Ø22 mm	Page 230
31	Weight of motor	15 g		0.5 - 1.0 Nm	
Values listed in the table are nominal.					
Connection		with hall sensors	sensorless		
Pin 1	4.5 ... 24 VDC	Motor winding 1	Motor winding 1		
Pin 2	Hall sensor 3	Motor winding 2	Motor winding 2		
Pin 3	Hall sensor 1	Motor winding 3	Motor winding 3		
Pin 4	Hall sensor 2	neutral point			
Pin 5	GND				
Pin 6	Motor winding 3				
Pin 7	Motor winding 2				
Pin 8	Motor winding 1				
Adapter		Order number			
see p. 299		220300			
Connector		Article number			
AMP		1-487951-1	487951-4		
MOLEX		52207-1190	52207-0490		
MOLEX		52089-1110	52089-0410		
Pin for design with Hall sensors: FPC, 11 pole, pitch 1.0 mm, top contact style Wiring diagram for Hall sensors see page 29					

B Friction calculations

B1 φ -part

The friction in deep groove ball bearings can be approximated with a constant friction coefficient $\mu = 0,0015$ [8]. This approximation holds when the following conditions are met:

- normal operating conditions
- well lubricated
- $P \approx 0,1 \cdot C$ (P = bearing load and C = load capacity)

Then, the friction torque T_f is given by:

$$T_f = \mu \cdot F \cdot \frac{d_m}{2} \quad (\text{B.1})$$

With:

$$d_m = \frac{d_o + d_i}{2} \quad (\text{B.2})$$

d_o = outer bearing diameter

d_i = inner bearing diameter

The friction of the two ball bearings that hold the φ -shaft is approximated by using the load $F = 5$ N in z direction at the pen (appendix C). This load generates a load on the front bearing $F_2 = 12$ N and on the back bearing $F_1 = 7$ N. The front bearing is a SKF 69102 ($d_i = 15$ mm, $d_o = 28$ mm, $w = 7$ mm) and the back bearing is a SKF 69101 ($d_i = 12$ mm, $d_o = 24$ mm, $w = 6$ mm).

$$T_{f,front} = 2 \cdot 10^{-4} \text{ Nm}$$

$$T_{f,back} = 1 \cdot 10^{-4} \text{ Nm}$$

B2 ψ -part

The only difference in the ψ part is the different load on the bearings. With the same z load of 5 N, $F_1 = 6$ N and $F_2 = 1$ N. This leads to a friction torque of:

$$\Rightarrow T_{f,front} = 1 \cdot 10^{-4} Nm$$

$$\Rightarrow T_{f,back} = 1 \cdot 10^{-5} Nm$$

B3 Z-friction

The friction in z is created by the 2 rotation/translation bearings, the 3 ball grooves, rack guiding, gear meshing, motor bearings and encoder.

The rotation/translation bearing friction is modeled by:

$$F_{f,trans} = \mu \cdot F \quad (B.3)$$

With the values used at the θ friction for the bearings:

$$\Rightarrow F_{f,trans} = 0,1N$$

The groove friction is measured to be 0,05 N.

The rack guiding contains 4 deep groove ball bearings, reference number 618 ($d_i = 1,5$ mm, $d_o = 4$ mm, $w = 1,2$ mm). These bearings are loaded by approximately 2 N, caused by the pressure angle of the rack pinion transmission. With B.1 this generates a friction torque, acting in z direction according to B.3. With $\mu = 0,0015$:

$$\Rightarrow F_{f,rack} = 8 \cdot 10^{-3} N$$

The gear meshing is calculated by 4.17.

$$\Rightarrow F_{f,gear} = 0,1N$$

The motor bearing friction is approximated by using two deep groove ball bearings ($d_i = 3$ mm, $d_o = 10$ mm, $w = 4$ mm), loaded in z with 5 N resulting in $F_1 = 6$ N and $F_2 = 1$ N load on the front and back bearing (appendix C). With B.1:

$$\Rightarrow T_{f,m} = 7 \cdot 10^{-5} Nm$$

The encoder friction is given by (appendix A):

$$\Rightarrow T_{f,e} < 3 \cdot 10^{-3} Nm$$

Measurement of the motor shaft, with encoder mounted on the back leads to a friction torque of:

$$\Rightarrow T_{f,m+e} = 7 \cdot 10^{-5} Nm$$

B4 θ -friction

The friction in θ is created by the 2 rotation/translation bearings, z-rollers, gear meshing, motor bearings and encoder.

The rotation/translation bearing friction is modeled by B1. A light pretension is used, therefore $\mu \approx 0,002$ [14]. The friction is approximated by the maximum load of 10 N in φ and ψ direction, generating a load of $F_2 = 30 N$ and $F_1 = 20 N$ on the lower and upper bearing. With:

$$d_m = 1,2 \cdot 10^{-2} m$$

$$\Rightarrow T_{f,rot} = 6 \cdot 10^{-4} Nm$$

The z rollers are 2 deep groove ball bearings, reference number 618 ($d_i = 1,5 mm$, $d_o = 4 mm$, $w = 1,2 mm$). These bearings are loaded by 10 N and generate a friction torque according to B.1. For each bearing, at its d_o this can be seen as a force working on a radius $r_z = 7 mm$ (figure 4.9). The z-roller friction is given by:

$$\Rightarrow T_{f,z-rolls} = 2 \cdot 10^{-4} Nm$$

The gear meshing is calculated by 4.23.

$$\Rightarrow T_{f,gear} = 1 \cdot 10^{-3} Nm$$

The motor bearing friction together with the encoder friction is measured to be:

$$\Rightarrow T_{f,m+e} = 7 \cdot 10^{-5} Nm$$

B5 Button part

In the button part miniature deep groove ball bearings are used. The two button bearings are Brammer XXX ($d_i = 1,5 mm$, $d_o = 4 mm$, $w = 1,2 mm$). The bearings in the motor are approximated by the same bearings. With the maximum button force of $F = 5 N$, the maximum bearing is loaded with 2 N, giving a maximum bearing friction of:

$$\Rightarrow T_{f,b} \approx T_{f,m} \approx 6 \cdot 10^{-6} Nm$$

C Stiffness calculations

Most stiffness's are not directly proportional to the applied force. Therefore, one can not always speak of 'the stiffness', only of a 'local stiffness' $dF/d\delta$. The continuous forces and torques offered to the surgeon's hand in each direction (table 3.1) are taken as load to determine this local stiffness. To make a fair comparison, the stiffness of each part is determined by evaluating the displacement of the surgeons hand due to this load.

In tableC.1 the evaluated stiffness's in their direction of interest are stated. Some parts were expected to be of no importance of the total stiffness on forearm. For completeness all parts of the stiffness chain are discussed, in the order of the table.

Table C.1: Stiffness haptic pen parts

Part	Material*	c_z [N/m]	k_θ [Nm/rad]	c_φ [N/m]	c_ψ [N/m]
<i>z- bush rim</i>	AlMgSi1	$2 \cdot 10^7$			
<i>z-roller</i>	SS304	$2 \cdot 10^6$			
<i>z-roller axle</i>	SS304	$5 \cdot 10^7$			
<i>rack</i>	CuZn39Pb3	$6 \cdot 10^7$			
<i>ball groove</i>	SS1.4112		$4 \cdot 10^2$		
<i>θ-z bush</i>	SS1.3505	$4 \cdot 10^8$	$3 \cdot 10^3$		
<i>tooth meshing</i>	SS303	$1 \cdot 10^7$	$4 \cdot 10^3$		
<i>motor shaft</i>	SS304	$2 \cdot 10^6$	$1 \cdot 10^2$		
<i>motor bearings</i>	SS1.3505	$3 \cdot 10^6$	$1 \cdot 10^3$		
<i>motor suspension</i>	AlMgSi1	$3 \cdot 10^7$	$1 \cdot 10^4$		
<i>ψ shaft</i>	SS304	$2 \cdot 10^8$	$5 \cdot 10^3$	$7 \cdot 10^5$	$2 \cdot 10^8$
<i>φ shaft</i>	SS304	$5 \cdot 10^6$	$5 \cdot 10^3$	$5 \cdot 10^6$	$7 \cdot 10^5$
<i>ψ bearings</i>	SS1.3505	$3 \cdot 10^6$	$4 \cdot 10^2$	$1 \cdot 10^6$	$3 \cdot 10^6$
<i>φ bearings</i>	SS1.3505	$6 \cdot 10^5$	$3 \cdot 10^3$	$6 \cdot 10^5$	$1 \cdot 10^6$
<i>ψ house</i>	AlMgSi1	$3 \cdot 10^5$	$7 \cdot 10^3$	$1 \cdot 10^7$	$2 \cdot 10^7$
<i>φ house</i>	AlMgSi1	$2 \cdot 10^6$	$6 \cdot 10^3$	$2 \cdot 10^6$	$5 \cdot 10^5$
<i>φ-ψ link</i>	AlMgSi1	$2 \cdot 10^7$	$4 \cdot 10^3$	$3 \cdot 10^6$	$5 \cdot 10^6$
<i>rot/tr bearing</i>	SS1.3505			$7 \cdot 10^5$	$3 \cdot 10^6$
<i>θ-z shaft</i>	SS1.3505			$7 \cdot 10^5$	$7 \cdot 10^5$

* SS = stainless steel

All parts are made of aluminum, brass or steel. The Young's moduli for the different steel types do not differ much. The following moduli for the 3 materials are used:

$$E_{steel} = 210 \cdot 10^9 \text{ N / m}^2$$

$$E_{al} = 70 \cdot 10^9 \text{ N / m}^2$$

$$E_{brass} = 100 \cdot 10^9 \text{ N / m}^2$$

z-bush rim

The bush rim is modeled with FEM (finite element method in NX3.0), see figure C.1.

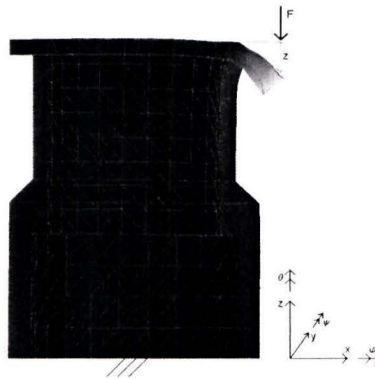


Figure C.1: z-bush rim

With:

$$F = 5 \text{ N}$$

$$z = 3 \cdot 10^{-7} \text{ m}$$

$$\Rightarrow c_z = 1,7 \cdot 10^7 \text{ N / m}$$

Z-rollers

The radial stiffness of the rollers is directly felt in z-direction. It is based on extrapolation of the bearing stiffness table [5] with shaft diameter d (figure C.2).

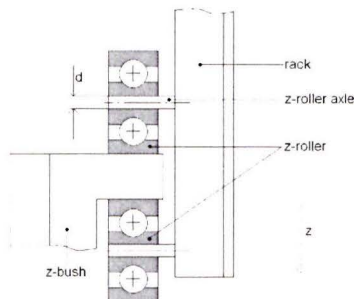


Figure C.2: z-roller and z-roller axle

$$\begin{aligned}
F &= 1N \\
d &= 1,5 \cdot 10^{-3} m \\
\Rightarrow c_z &= 2 \cdot 10^6 N / m
\end{aligned}$$

Z-roller axle

The roller axle is modeled as a wire spring, connected to the fixed world (rack) at one end (figure C.2). The stiffness in z direction is given by (4.16):

$$\begin{aligned}
d &= 1,5 \cdot 10^{-3} m \\
l &= 1,6 \cdot 10^{-3} m \\
\Rightarrow c_z &= 5 \cdot 10^7 N / m
\end{aligned}$$

Rack

The rack has a variable distance from tooth meshing to roller axle (contact stiffness of tooth meshing will be discussed later in this paragraph). The largest occurring length is considered, because this gives the lowest stiffness in z direction, by:

$$c_z = \frac{EA}{l} \quad (C.1)$$

$$\begin{aligned}
A &= 2,4 \cdot 10^{-5} m^2 \\
l &= 3 \cdot 10^{-2} m \\
\Rightarrow c_z &= 6 \cdot 10^7 N / m
\end{aligned}$$

Ball groove

The ball groove consists of 9 balls with radius r in 3 grooves with pitch circle diameter d_p . For a hardened steel ball pressed on a hardened steel plate with force F the following holds for the compression δ (difference between distance of ball centre to plate before and after deformation):

$$\delta = 3,5 \cdot 10^{-4} \left(F^2 / 1000 \cdot r \right)^{1/3} \quad (C.2)$$

Each ball is loaded by:

$$F = \frac{\frac{1}{9} T_{peak}}{\frac{1}{2} d_p} \quad (C.3)$$

The total torsional stiffness k_θ of the 9 balls is given by:

$$k_\theta = \left(\frac{1}{2} d_p \right)^2 \frac{9F}{\delta} \quad (C.4)$$

Assuming that the load, manufacturing precision of the grooves and roundness of the balls is high enough to let all balls be compressed. With:

$$\begin{aligned} T_{peak} &= 50 \cdot 10^{-3} \text{ Nm} \\ d_p &= 1,8 \cdot 10^{-2} \text{ m} \\ \Rightarrow k_\theta &= 2 \cdot 10^3 \text{ Nm / rad} \end{aligned}$$

In the worst case scenario only one ball is compressed, the stiffness is then given by:

$$k_\theta = 4 \cdot 10^2 \text{ Nm / rad}$$

θ -z bush

The z stiffness of a θ -z bush is calculated with (C.1), where the area A is given by:

$$A = \frac{\pi}{4} (d_o^2 - d_i^2) \quad (\text{C.5})$$

$$\begin{aligned} d_o &= 3,6 \cdot 10^{-2} \text{ m} \\ d_i &= 1,5 \cdot 10^{-2} \text{ m} \\ \Rightarrow c_z &= 4 \cdot 10^8 \text{ N / m} \end{aligned}$$

The torsional stiffness given by:

$$k = \frac{GI_p}{l} \quad (\text{C.6})$$

$$I_p = \frac{\pi}{32} (d_o^4 - d_i^4) \quad (\text{C.7})$$

$$\begin{aligned} G &\approx 0,385 \cdot E \\ l &= 1,5 \cdot 10^{-1} \text{ m} \\ \Rightarrow k_\theta &= 3 \cdot 10^3 \text{ Nm / rad} \end{aligned}$$

Tooth meshing

There are two tooth meshes, for the z translation and for the θ rotation. Both meshes have almost the same geometry (same module m). The tooth bending stiffness and tooth contact stiffness together form the total tooth stiffness. The tooth bending is modeled like a leaf spring, loaded from the tip (figure C.2).

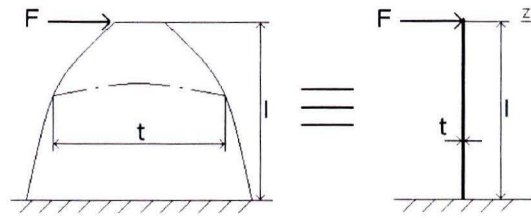


Figure C.2: tooth bending

The stiffness in z direction is given by:

$$c_z = \frac{Eht^3}{4l^3} \quad (C.8)$$

$$l \approx 2 \cdot m \quad \text{from [6]} \quad (C.9)$$

$$t \approx \pi \cdot m / 2 \quad \text{from [6]} \quad (C.10)$$

$$m = 0,3$$

$$h = 1 \cdot 10^{-3} m$$

$$\Rightarrow c_{bend} = 1 \cdot 10^8 N / m \text{ for each tooth}$$

The contact stiffness is modeled like the stiffness of a cylinder in contact with a flat plate, both made of hardened steel. For this contact the following holds [5]:

$$\delta = 3,75 F^{0,9} / (10^5 l^{0,8}) \quad (C.11)$$

$$c = \frac{F}{\delta} \quad (C.12)$$

With:

$$F = 5 N$$

$$l = 1 \cdot 10^{-3} m$$

$$\Rightarrow c_{cont} = 2 \cdot 10^7 N / m$$

The stiffness for two teeth in mesh (according to 4.31) is:

$$\frac{1}{c_z} = \frac{2}{c_{bend}} + \frac{1}{c_{cont}} \quad (C.13)$$

$$\Rightarrow c_z = 1 \cdot 10^7 N / m$$

The θ rotational stiffness is given by:

$$k_\theta = c_z \cdot r^2 \quad (C.14)$$

With:

$$r = 2 \cdot 10^{-2} m$$

$$\Rightarrow k_\theta = 4 \cdot 10^3 Nm / rad$$

Motor shaft

The motor shaft stiffness is divided in bending and torsion of the shaft. The load case of the bending of the shaft is given by figure C.3. The bending of the shaft in z and θ is divided in two parts, the bending of the front end of the shaft and the bending of the shaft between its bearings, causing an angular movement of the front end of the shaft (figure C.4).

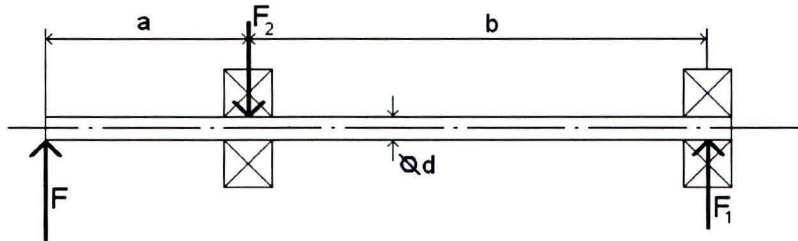


Figure C.3: load case of motor shaft

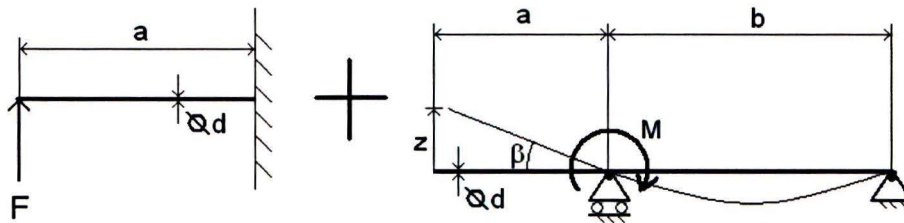


Figure C.4: Front end bending (left) and between bearings bending (right)

The bending stiffness of the front end, $c_{b,f}$, is given by [9]:

$$c_{b,f} = 0,15 \frac{Ed^4}{a^3} \quad (C.15)$$

The bending stiffness of the shaft between the bearings, $c_{b,b}$, is given by:

$$\beta = \frac{M \cdot b}{3EI} \quad (C.16)$$

where:

$$M = F \cdot a \quad (C.17)$$

$$I = \frac{\pi}{64} d^4 \quad (C.18)$$

$$z = \beta \cdot a \quad (C.19)$$

Which gives:

$$c_{b,b} = \frac{F}{z} \quad (C.20)$$

These bending stiffnesses can be transformed to torsional stiffnesses (in θ), given by C.14, where $r = 5,7 \cdot 10^{-3} m$.

The torsional stiffness is given by C.6, where:

$$I = \frac{\pi d^4}{32} \quad (\text{C.21})$$

This torsional stiffness can be transformed to a translational stiffness (in z), also given by C.14 with $r = 2 \cdot 10^{-2} m$.

The all these stiffnesses added up for the θ and z direction separately according to equation 4.37 on p.41 gives:

$$F = 5N$$

$$a = 5 \cdot 10^{-3} m$$

$$b = 5 \cdot 10^{-2} m$$

$$d = 3 \cdot 10^{-3} m$$

$$l = a + \frac{b}{2}$$

$$\Rightarrow c_z = 2 \cdot 10^6 N / m$$

$$\Rightarrow k_\theta = 8 \cdot 10^2 Nm / rad$$

Bearing stiffness

In figure 4.4 on p.17 a simplified version of figure C.3 is shown. The radial stiffness of the bearings is represented by two springs, with stiffness c_1 and c_2 . The substitute stiffness, c_s , is the stiffness felt at the position of force F , given by:

$$c_s = \frac{F}{z_3} \quad (\text{C.22})$$

$$z_3 = \frac{a}{b} z_1 + \frac{a+b}{b} z_2 \quad (\text{C.23})$$

$$z_1 = \frac{F_1}{c_1} \quad (\text{C.24})$$

$$z_2 = \frac{F_2}{c_2} \quad (\text{C.25})$$

$$\sum M = 0 \quad (\text{C.26})$$

$$\sum F = 0 \quad (\text{C.27})$$

$$F_1 = \frac{a}{b} F \quad (\text{C.28})$$

$$F_2 = \frac{a+b}{b} F \quad (\text{C.29})$$

$$\Rightarrow \frac{1}{c_s} = \frac{\left(\frac{a}{b}\right)^2}{c_1} + \frac{\left(\frac{a+b}{b}\right)^2}{c_2} \quad (\text{C.30})$$

With:

$$c_1 = c_2 = 4 \cdot 10^6 \text{ N / m}$$

$$\Rightarrow c_z = 3,3 \cdot 10^6 \text{ N / m}$$

$$\Rightarrow k_\theta = 1,3 \cdot 10^3 \text{ Nm / rad (according to C.14)}$$

Motor suspension

The suspension is modeled with FEM (figure C.6). The stiffness in z is given by:

$$F = 2,5 \text{ N}$$

$$z = 2 \cdot 10^{-7} \text{ m}$$

$$\Rightarrow c_z = 2,5 \cdot 10^7 \text{ N / m}$$

In θ the suspension stiffness is approximately the same. Converted to torsional stiffness by C.14:

$$r = 2 \cdot 10^{-2} \text{ m}$$

$$\Rightarrow k_\theta = 1 \cdot 10^4 \text{ Nm / rad}$$

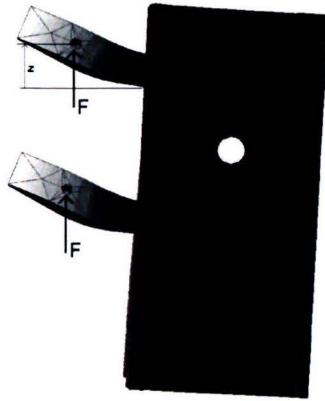


Figure C.6: motor suspension

ψ -shaft

The stiffness of the ψ -shaft is determined by the bending of the shaft between the bearings and the torsion of the shaft. The bending of the front end of the shaft is neglected. The stiffnesses in φ , θ and z direction are determined by a load on the shaft causing only bending, while in ψ directions also torsion of the shaft occurs, causing a lower stiffness.

Bending stiffness in φ , ψ and z is determined by C.16:

$$\begin{aligned}
 F &= 5N \\
 a &= 1,2 \cdot 10^{-2} m \\
 b &= 4,2 \cdot 10^{-2} m \\
 d &= 1,2 \cdot 10^{-2} m \\
 \Rightarrow c_{\psi/z} &= 1,8 \cdot 10^8 N / m
 \end{aligned}$$

Bending stiffness in θ is determined by:

$$k_{\theta} = \frac{M}{\beta} \quad (C.31)$$

$$\beta = \frac{M \cdot l}{EI} \quad (C.32)$$

where M is given by C.15.

$$\Rightarrow k_{\theta} = 5 \cdot 10^3 Nm / rad$$

Torsion is the limiting stiffness in ψ direction and determined by C.3 and C.4. With C.14 the torsional stiffness is transformed to linear stiffness with:

$$\begin{aligned}
 r &= 1,5 \cdot 10^{-1} m \\
 \Rightarrow c_{\varphi} &= 7 \cdot 10^5 N / m
 \end{aligned}$$

φ -shaft

The φ -shaft stiffness is analogue to the ψ -shaft, only φ and ψ are switched and the parameters a and b are changed in:

$$\begin{aligned}a &= 5,6 \cdot 10^{-3} \text{ m} \\b &= 3,9 \cdot 10^{-2} \text{ m} \\ \Rightarrow c_{\varphi/z} &= 5 \cdot 10^6 \text{ N / m} \\ \Rightarrow k_{\theta} &= 5 \cdot 10^3 \text{ Nm / rad} \\ \Rightarrow c_{\psi} &= 7 \cdot 10^5 \text{ N / m}\end{aligned}$$

ψ -bearings

The ψ -bearing stiffness in ψ and z direction is determined by 4.6, 4.7, 4.8 and 4.9, with:

$$\begin{aligned}\alpha &= 20^\circ \\d_m &= 20 \cdot 10^{-3} \text{ m} \\a &= 12 \cdot 10^{-3} \text{ m} \\b &= 42 \cdot 10^{-3} \text{ m} \\c_1 = c_2 &= 6 \cdot 10^6 \text{ N / m} \\ \Rightarrow c_{\psi/z} &= 3 \cdot 10^6 \text{ N / m}\end{aligned}$$

For the θ direction, the torsional stiffness is determined by C.14 with:

$$\begin{aligned}r &= a \\ \Rightarrow k_{\theta} &= 4 \cdot 10^2 \text{ Nm / rad}\end{aligned}$$

In φ direction also the axial stiffness of the bearings has influence on the total stiffness and from [5] this is:

$$c_{axial} = 2 \cdot 10^6 \text{ N / m}$$

$$\Rightarrow c_{\varphi} = 1 \cdot 10^6 \text{ N / m}$$

φ -bearings

The φ bearings stiffness is analogue to the ψ bearings, only φ and ψ are switched and a and b are changed:

$$a = 56 \cdot 10^{-3} \text{ m}$$

$$b = 39 \cdot 10^{-3} \text{ m}$$

$$\Rightarrow c_{\varphi/z} = 6 \cdot 10^5 \text{ N / m}$$

$$\Rightarrow c_{\psi} = 1 \cdot 10^6 \text{ N / m}$$

$$\Rightarrow k_{\theta} = 2,5 \cdot 10^3 \text{ Nm / rad}$$

ψ -house

The ψ house is modeled with FEM (figure C.7). In the front view the positions is shown where the housing is fixed.

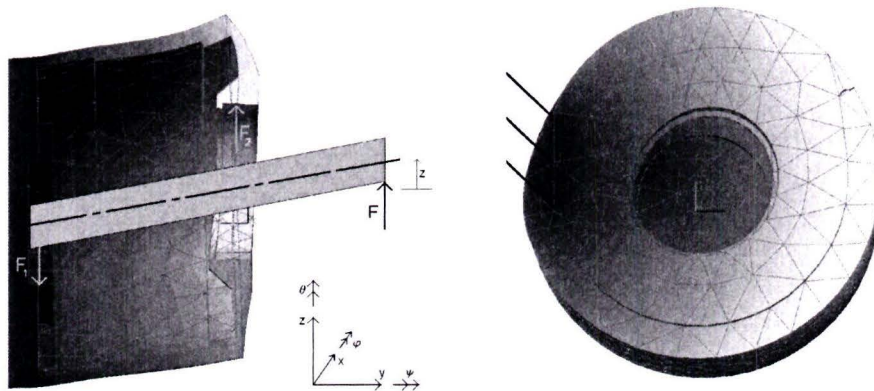


Figure C.7: φ house cross section and front view

The forces F_1 and F_2 are calculated by C.24 and C.25. This gives stiffness in z :

$$F = 5 \text{ N}$$

$$z = 1 \cdot 10^{-7} \text{ m}$$

$$\Rightarrow c_z = 2,5 \cdot 10^7 \text{ N / m}$$

In ψ direction the bearing load is of the same magnitude, only the direction is changed leading to:

$$z = 3 \cdot 10^{-7} \text{ m}$$

$$\Rightarrow c_{\psi} = 2 \cdot 10^7 \text{ N / m}$$

In φ direction the same stiffness as in z direction occurs, only the 'felt' stiffness at the surgeons hand is factor b/l smaller.

$$\begin{aligned} b &= 42 \cdot 10^{-3} \text{ m} \\ l &= 1,5 \cdot 10^{-1} \text{ m} \\ \Rightarrow c_{\varphi} &= 1 \cdot 10^7 \text{ N / m} \end{aligned}$$

The θ stiffness is determined by C.14:

$$\begin{aligned} r &= a \\ a &= 12 \cdot 10^{-3} \text{ m} \\ \Rightarrow k_{\theta} &= 7 \cdot 10^3 \text{ Nm / rad} \end{aligned}$$

φ -house

The φ house and fixed world are loaded similar to the ψ house (figure C.7). The difference is in boundary conditions. It is modeled with FEM (figure C.8).

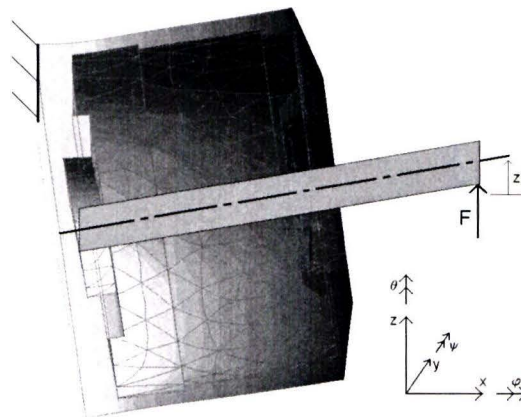


Figure C.8: φ house cross section

The z stiffness of the φ house is given by:

$$\begin{aligned} F &= 5 \text{ N} \\ z &= 2 \cdot 10^{-6} \text{ m} \\ \Rightarrow c_z &= 2 \cdot 10^6 \text{ N / m} \end{aligned}$$

In φ direction the bearing loads have the same magnitude and z is the same, only the direction is changed.

$$\Rightarrow c_{\varphi} = 2 \cdot 10^6 \text{ N / m}$$

In ψ direction the same stiffness as in z direction occurs, only the stiffness at the surgeons hand is factor b/l smaller.

$$\begin{aligned} b &= 39 \cdot 10^{-3} \text{ m} \\ l &= 1,5 \cdot 10^{-1} \text{ m} \\ \Rightarrow c_{\psi} &= 5 \cdot 10^5 \text{ N / m} \end{aligned}$$

The θ stiffness is determined by C.14 with:

$$\begin{aligned} r &= a \\ a &= 56 \cdot 10^{-3} \text{ m} \\ \Rightarrow k_{\theta} &= 6 \cdot 10^3 \text{ Nm / rad} \end{aligned}$$

ϕ - ψ -link

The ϕ - ψ link is modeled with FEM. An body which has significantly higher stiffness than the link, is added to apply the forces on the link (figure C.9).

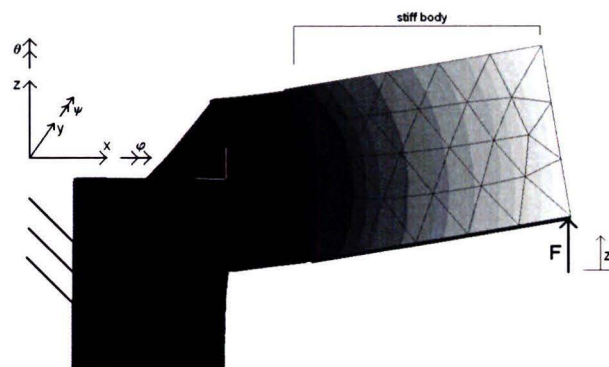


Figure C.9: ϕ - ψ link

The z stiffness of the ϕ - ψ -link is given by:

$$\begin{aligned} F &= 5 \text{ N} \\ z &= 3 \cdot 10^{-7} \text{ m} \\ \Rightarrow c_z &= 2 \cdot 10^7 \text{ N / m} \end{aligned}$$

In ψ direction the same stiffness as in z direction occurs, only the stiffness at the surgeons hand is factor b/l smaller.

$$\begin{aligned} b &= 35 \cdot 10^{-3} \text{ m} \\ l &= 1,5 \cdot 10^{-1} \text{ m} \\ \Rightarrow c_{\psi} &= 5 \cdot 10^6 \text{ N / m} \end{aligned}$$

In φ direction a moment about φ is applied at the same position of the force. This results in a displacement at the surgeons hand. The stiffness is calculated with:

$$\begin{aligned} M &= F \cdot r = 5 \cdot 0,15 = 0,75 Nm \\ z &= 1,7 \cdot 10^{-6} m \\ \Rightarrow c_{\varphi} &= 3 \cdot 10^6 N / m \end{aligned}$$

The θ stiffness is approximated by C.14 using c_{φ} :

$$\begin{aligned} r &= b \\ \Rightarrow k_{\theta} &= 3,7 \cdot 10^3 Nm / rad \end{aligned}$$

Rotation/translation bearings

The θ -z bearing stiffness is felt in φ and ψ direction. The stiffness of the bushes is approximated by comparing the static load capacity of the bushes with that of a deep groove ball bearing. A ball bearing with $d_{in} = 5 mm$ matches with each bush. The stiffness of each bush is determined by [5]. The substitute stiffness in φ and ψ is given by C.26, and calculated in 4.2.3.

θ -z axle

The bending stiffness of the θ -z axle is felt in φ and ψ direction and given by:

$$c = \frac{72 EI}{5 l^3} \quad (C.33)$$

where I is given by C.6. With:

$$\begin{aligned} l &= 1,5 \cdot 10^{-1} m \\ d_o &= 1 \cdot 10^{-2} m \\ d_i &= 7 \cdot 10^{-3} m \\ \Rightarrow c_{\varphi/\psi} &= 7 \cdot 10^5 N / m \end{aligned}$$

D Cable wrapping

In figure D.1 a cross section of a flat flexible cable (FFC) segment with three conductors is shown.

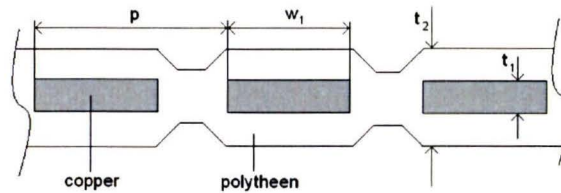


Figure D1: cross section flexible flat cable

D1 ϕ and ψ cable wrapping

To keep the total width within 25 mm for compactness, two cables with together 66 conductors are necessary for connection of the motors and encoders of the button, θ -z and ψ part. The two cables will be wound up like a spiral, shown in figure D.2.

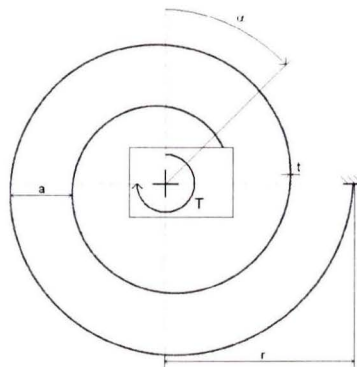


Figure D.2: spiral spring

The cables are modeled like a spiral spring where its torque is given by:

$$T = \frac{\alpha \cdot wt^3 E}{12l_c} \quad (D.1)$$

The length of the cable (l_c) is determined empirically, together with the number of windings (n). The cable is wind up around the encoder ($r_e = 12 \text{ mm}$) and within the cable cover ($r_c = 25 \text{ mm}$). With the total stroke of $\alpha = \pm 90^\circ$ the cable should not touch the encoder or cover, giving:

$$l_c = 0,3m$$

$$n = 2$$

The cables consist of two different materials with different Young's moduli E . The total torque is approximated by determining the torques for each material separately. For the copper part the following sizes are taken:

$$w = 66 \cdot w_1 = 66 \cdot 3 \cdot 10^{-4} = 20 \cdot 10^{-3} m ,$$

$$t = t_1 = 1 \cdot 10^{-4} m ,$$

while

$$E_{copper} = 120 \cdot 10^9 \text{ N / m}^2$$

And for the polytheen part:

$$w = 66 \cdot p = 66 \cdot 5 \cdot 10^{-4} = 3 \cdot 10^{-2} m ,$$

$$t = t_2 = 3 \cdot 10^{-4} m ,$$

while

$$E_{polytheen} = 0,5 \cdot 10^9 \text{ N / m}^2$$

The maximum disturbance torques the cable generates is given by:

$$\Rightarrow T_{copper} = 1 \cdot 10^{-3} \text{ Nm}$$

$$\Rightarrow T_{polytheen} = 2 \cdot 10^{-4} \text{ Nm}$$

$$\Rightarrow T_{cable} = 1 \cdot 10^{-3} \text{ Nm}$$

At the hand of the surgeon at distance $l = 150 \text{ mm}$, this gives:

$$F_{cable} = \frac{T_{cable}}{l} = 7 \cdot 10^{-3} \text{ N} \quad \text{(D.2)}$$

The cycle life of a FFC is given in figure D.3 [11].

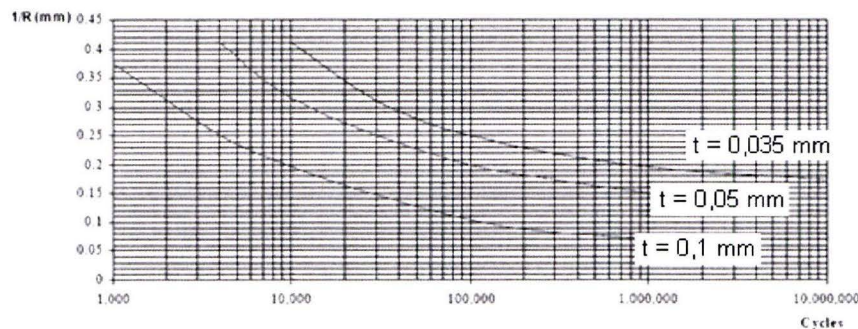


Figure D.3: cycle life in relation to the bending radius.

From figure D.3 it can be seen that the cycle life for an FFC with bending radius $r_c = 12\text{mm}$ is over 10^6 cycles for all cable thicknesses. This will be enough.

D2 θ -z cable wrapping

The cable for the connection of the button motor and encoder has a width of 10 mm and has 10 conductors. The cable is coiled in a similar way the φ and ψ cables are and the θ movement of the cable is also similar to the φ and ψ movement. Its minimum bending radius is determined by the tube with $r_i = 5\text{ mm}$ and its maximum radius is determined by the θ -z block, with $r_o = 13\text{ mm}$ (figure D.4). With the total stroke of $\alpha = \pm 175^\circ$ the cable should not touch the encoder or cover, giving:

$$l_c = 9 \cdot 10^{-2} \text{ m}$$

$$n = 3$$

In θ this gives a maximum disturbance force with (D1):

For the copper part:

$$w = 10 \cdot w_1 = 10 \cdot 3 \cdot 10^{-4} = 3 \cdot 10^{-3} \text{ m}$$

$$t = t_1 = 1 \cdot 10^{-4} \text{ m}$$

For the polyetheten part:

$$w = 10 \cdot p = 10 \cdot 5 \cdot 10^{-4} = 5 \cdot 10^{-3} \text{ m}$$

$$t = t_2 = 3 \cdot 10^{-4} \text{ m}$$

Together gives:

$$\Rightarrow T_{cable,\theta} = 1 \cdot 10^{-3} \text{ Nm}$$

A z-movement is added to the spiral spring. In the z direction the spring acts like a buffer spring (figure D.4).

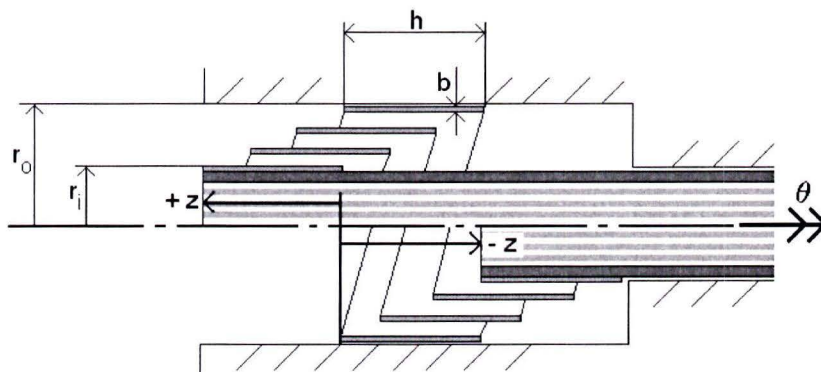


Figure D.4: z cable movement (tube and θ -z block aangeven)

Again, the total force is approximated by determining the force for each material separately. The disturbance force in z direction is given by [12]:

$$F_{cable,z} = \frac{2 \cdot k \cdot \frac{W}{t} \cdot t^4 \cdot G}{l_c (r_o^2 + r_i^2)} \cdot z \quad (D.3)$$

where k is a constant depending on h/b, G is the shear modulus and is approximated by:

$$G = 0,385 \cdot E$$

With:

$$k = 0,333$$

$$r_i = 2,5 \cdot 10^{-3} m$$

$$r_o = 6,5 \cdot 10^{-3} m$$

$$l_c = 9 \cdot 10^{-2} m$$

$$z = \pm 7,5 \cdot 10^{-3} m$$

$$\Rightarrow F_{cable,z} = 0,1 N$$

From figure D.3 the cycle life for the θ -z cable is approximately 1000 cycles. In this table one cycle means full bending and full unbending. However, in this case, full unbending will not take place, leading to a lower stress variation in the cable, leading to a higher cycle life. The cycle life will probably be enough.

E Tooth strength calculations

The tooth strength calculation comes from [13].

The load capacity of the gear is based on AGMA 2001-B88 and the following assumptions have been made:

- the gears are simply supported in rolling element bearings
- pinion revolutions $>10^7$
- gears are grease lubricated
- reliability of 1 failure in 100 is acceptable

The basic load capacity (F_b) of a pair of spur gears is defined as the maximum tangential force at which they can operate indefinitely. F_b has two values: one calculated from tooth root strength, (F_{ts}), and one for tooth flank pitting (F_{tw}).

$$F_{ts} = 177,7 \cdot O \cdot w_f \cdot m \cdot K \cdot U_s \quad (\text{E.1})$$

$$F_{tw} = 14,64 \cdot N \cdot L \cdot w_f \cdot m \cdot K \cdot U_w \quad (\text{E.2})$$

With:

$$K = \left(\frac{84}{84 + \sqrt{200v_t}} \right)^{0,4} \quad (\text{E.3})$$

$$v_t = \frac{rpm \cdot \pi \cdot N \cdot m}{60000} \quad (\text{E.4})$$

N = number of teeth

O = geometry factor, strength

L = geometry factor, wear

w_f = face width of smallest gear

m = module

K = dynamic factor

v_t = pitch line velocity

U_s = material strength modification factor

U_w = material wear modification factor

Both calculations should be made and the lower value used.

E1 Z-drive

In the rack and pinion transmission, the pinion is the weakest link:

- $N = 38 \text{ teeth}$
- $w_f = 1,5 \text{ mm}$
- $m = 0,3$
- $\text{rpm} = 60 \text{ revolutions per minute}$ (z move of approximately 1 Hz)
- $O = 0,42$ (figure E.1A, rack is modeled like gear with 10^3 teeth)
- $L = 0,12$ (figure E.1B, rack is modeled like gear with 10^3 teeth)
- $U_s = 0,43$ (table E.1)
- $U_w = 0,15$ (table E.1)
- $\Rightarrow F_{Is} = 14N$
- $\Rightarrow F_{Iw} = 4,5N$

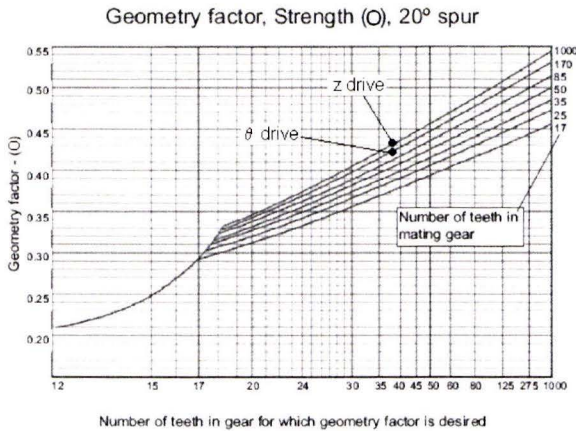


Figure E.1A: geometry factor J

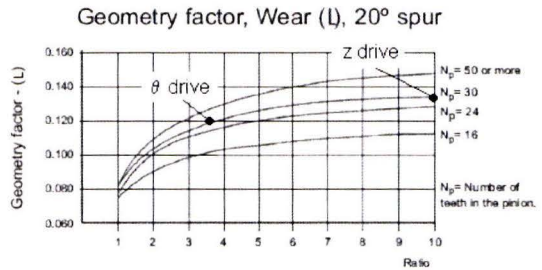


Figure E.1B: geometry factor I

Table E.1 Gear material modification factors

Material	Specification	Strength	Wear
Hardened Stainless steel	17-4PH	1.00	1.00
Stainless steel	303S31	0.43	0.15
Stainless steel	316S31	0.47	0.20
Aluminium alloy	L168	0.37	0.10
Brass	CZ121	0.35	0.13

E2 θ -drive

Again, the pinion is the weakest link. The only difference with the z pinion calculation is the geometry factor for wear ($L = 0,135$) and strength ($J = 0,44$), see figure E.1.

$$\Rightarrow F_{ts} = 15N$$

$$\Rightarrow F_{tw} = 5N$$

With $r_p = 5,7 \cdot 10^{-3} m$, this gives:

$$\Rightarrow T_{ts} = 8,6 \cdot 10^{-2} Nm$$

$$\Rightarrow T_{tw} = 2,9 \cdot 10^{-2} Nm$$

F Angular button acceleration

The button acceleration is based on one full press and release in 1 s; a 1 Hz movement. A schematic view of the buttond is shown in figure F.1.

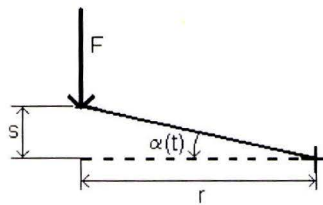


Figure F.1: button pressing

The angular acceleration of the button can be determined by:

$$\alpha_{\max} \approx \tan^{-1} \left(\frac{s_{\max}}{r_b} \right) \quad (\text{F.1})$$

$$\alpha(t) = \frac{1}{2} \alpha_{\max} \sin(2\pi ft) \quad (\text{F.2})$$

$$\ddot{\alpha}_{\max} = \frac{1}{2} \alpha_{\max} (2\pi f)^2 \quad (\text{F.3})$$

With:

$$\text{freq} = 1\text{Hz}$$

$$s = 5 \cdot 10^{-3} \text{m}$$

$$r_b = 2 \cdot 10^{-2} \text{m}$$

$$\Rightarrow \ddot{\alpha}_{\max} = 0,67 \text{rad} / \text{s}^2$$

List of symbols

<i>Symbol</i>	<i>Description</i>	<i>Unit</i>
α	angle	rad or °
$\dot{\alpha}$	angular velocity	rad/s
$\ddot{\alpha}$	angular acceleration	rad/s ²
β	angle	rad or °
δ	compression	m
η	efficiency	-
θ	angle	rad or °
ρ	density	kg/m ³
σ	stress	N/m ²
μ	friction coefficient	-
φ	angle	rad or °
ψ	angle	rad or °
ω_n	eigen-frequency	Hz

<i>Symbol</i>	<i>Description</i>	<i>Unit</i>
a	distance	m
A	area	m ²
b	distance	m
c	stiffness	N/m ²
C ₀	load capacity	N
C _{pt}	counts per turn	-
d	diameter	m
E	modulus of elasticity	N/m ²
f	deflection	m
F	force	N
g	gravity constant	m/s ²
G	shear modulus	N/m ²
h	height	m
i	ratio	-
I	second moment of area	m ⁴
J	inertia	kgm ²
k	rotational stiffness	Nm/rad
K	dynamic gear factor	-
l	length	m
L	geometry gear factor	-
m	mass	kg
m	module	m
M	moment	Nm
n	amount	-
O	geometry gear factor	-
p	pitch	m
P	load	N
Q	motor characteristic	kg/N
r	radius	m
rpm	revolutions per minute	-
R	resolution	m
s	distance	m
S _v	play	m
t	thickness	m
T	torque	Nm
U	gear material factor	-
v	velocity	m/s
w	width	m
W	friction force	N
X	position	m
y	position	m
z	position	m

Acknowledgement

Herewith, I would like to thank everybody who has helped me during my assignment. In the first place Nick Rosielle, for coaching and inspiring me during the last year. In the second place I would like to thank Ron Hendrix, my colleague in the Eye Rhas project and all the students from the Constructions and Mechanisms lab, helping me during the Monday-meetings. Finally I would like to thank my friends and family for their unconditional support.